Pergamon

Geochimica et Cosmochimica Acta, Vol. 66, No. 12, pp. 2211–2229, 2002

0016-7037/02 $22.00 + .00

PII S0016-7037(02)00905-5

On bimodal differentiation by solidification front instability in basaltic magmas, part 1: Basic mechanics

BRUCE D. MARSH*

Johns Hopkins University, M. K. Blaustein Department of Earth and Planetary Sciences, 34th and Charles Streets, Baltimore, MD 21218, USA

(*Received August* 13, 2001; *accepted in revised form March* 12, 2002)

Abstract—Extensive, coarse-grained silicic lenses are common in the upper portions of large diabase sills, lava lakes, and gabbroic intrusions. These lenses, which often contain up to 10 wt% more silica than their host rocks, record a clear process of bimodal differentiation that may play a fundamental role in generating significant quantities of silicic magma in predominantly basaltic systems. The spatial, compositional, textural, and contact relations suggest that these silicic segregations form by infilling of tears formed during gravitational instability of the upper solidification front. This process is investigated in some detail by exploring the thermal and mechanical conditions leading to internal failure of the front and segregation formation. As the upper solidification front grows inward and thickens, the local strength of the developing crystalline network must increase upward through the front sufficiently fast to offset the increasing weight of the front itself. This necessary local variation in strength dictates how crystallinity must vary to prevent failure. But the actual variation in crystallinity is determined by phase equilibria, which in general varies in a fashion that is noncovariant with that required for mechanical stability. It is this mismatch that apparently leads to failure and formation of silicic segregations. The rate of filling of the tears by porous flow of interstitial melt from below regulates the rate of tear opening, and the overall size of the tears is regulated by the local rate of advance of the solidification front. Segregations therefore thicken downward as the growth of the front slows and then die out altogether with approach of the lower solidification front. This process irreversibly introduces siliceous noise into basaltic systems. The silicic signal can be enhanced through subsequent reprocessing of the host rock to form volumetrically important masses of silicic magma. This process may be fundamental to achieving the strong compositional diversity of the igneous rocks, to yielding continental masses, and to the differentiation of Earth itself. *Copyright © 2002 Elsevier Science Ltd*

Field observations support the view that two magmas of highly contrasting compositions coexisted at least for limited periods and were erupted simultaneously throughout geologic time. The paucity of intermediate rocks casts doubt on the production of contrasting magmas by fractional crystallization. —H. S. Yoder, 1973

1. INTRODUCTION

That basaltic magma eventually gives rise to granitic magma through separation of crystals and melt is well established from a purely chemical perspective, but the physical process by which this happens is not at all clear. Crystal fractionation, in the usual sense of crystals sinking in a magma chamber, produces very limited enrichments of silica. Enormous piles of Hawaiian basalt, for example, showing no real sign of siliceous lava (e.g., dacite, rhyolite), are clear testimony to this inadequacy (Peterson and Moore, 1987; Marsh et al., 1991). It is thus unclear whether the so-called silica liquid line of descent, yielding andesites, dacites, and granites from basalt, is ever realized in the customary sense (e.g., Yoder, 1973) or is only achieved through repeated cycles of solidification and remelting. In this respect, the aim of the present study is to delineate a process of bimodal differentiation that may be of fundamental importance in producing silicic magma from basalt and also, on a larger scale, in generating protocontinental crust.

Perhaps the most unmistakable example of in situ bimodal differentiation is that of lenses of silicic or pegmatitic segregations commonly found at distinct horizons in the upper half of basaltic sills. The magnitude of silica enrichment in the segregations, as a measure of degree of differentiation, can be large; the bulk composition sometimes exceeds 70% (wt.) SiO_2 in diorite sills such as that at Stott Mountain, Oregon (MacLeod, 1981). More generally, however, segregation silica contents in basaltic (i.e., 50 to 55% silica) sills are in the range of 60 to 65% (e.g., Gunn, 1966). Long a subject of curiosity in sills (e.g., Walker, 1953), silicic segregations are also common in lava lakes (e.g., Richter and Moore, 1966; Wright and Okamura, 1977; Helz, 1980) and thick lava flows (e.g., Lindsley et al., 1970).

Silicic segregations are distinct over broadly similar, nonsilicic segregations, which also occur in the upper parts of some sills and lavas and are also often pegmatitic (e.g., Puffer and Horter, 1993; Carman, 1994; Philpotts et al., 1996). Nonsilicic segregations are characteristically enriched in Fe, Ti, K, P, Zr, Cu, Ba, and rare earth elements, depleted in Al, Ca, Mg, Ni, Cr, and Sr, but are unchanged over the host rock in silica and soda. Although this chemical contrast may reflect in some sills and lavas a fundamental difference in the bulk magma composition, which leads to a different differentiation sequence (e.g., Carman, 1994), these segregations are sometimes found in diabase sills of a bulk composition similar to those containing silicic segregations. They are also distinct in other ways. Nonsilicic segregations are often vesicular and the segregation texture coarsest in the middle of the lens and finer at both the upper and lower margins, quite unlike silicic segregations. The suggested origin of these nonsilicic segregations (e.g., Philpotts et al.,

* Author to whom correspondence should be addressed (bmarsh@jhu.edu).

1996) is also distinct over that suggested here for silicic segregations, as will be mentioned later. A concise overview of the characteristics of nonsilicic segregations, including their nomenclature and origin, is given by Puffer and Horter (1993), and Carman (1994) gives a similar overview for segregations in alkaline intrusion. Unless specifically noted, all further discussion and analysis here will concern only silicic segregations.

Although silicic segregations have often been mistaken as the so-called sandwich horizon of solidification, where the very last, most silicic melt has collected, it is clear from their chemical composition and distribution in bodies where the style of solidification is known that they are not sandwich melts. (In fact, it is not at all clear that the concept of "sandwich melts" has any physical meaning whatsoever.) In lava flows and sills, joints track the inward migration of the solid in the upper and lower solidification fronts, and the horizon of mismatched joints marks the true sandwich horizon. The silicic segregations always occur above this horizon and are most often best developed at some intermediate level between the middle or thermal sandwich horizon and the top of the body. In Hawaiian lava lakes, for example, they begin forming early in the formation of the upper crust, continue throughout most of the solidification history, and are absent in the true sandwich horizon (Helz, 1980).

In smaller bodies (~25 to 75 m), if present at all, the silicic segregations are generally long (1 to 2 m) and thin (1 to 5 cm), but in some thick (300 to 400 m) basaltic sills, they can attain thicknesses of 1 to 2 m and lengths of 40 to 50 m, often interdigitating to form a concentrated horizon of lenses. In other basaltic sills, typically nonquartz normative, of favorable size, they may be entirely absent, suggesting that magma chemical composition is an important factor in segregation formation.

A surprising feature of segregation-bearing sills is the repeated presence of unusually abundant siliceous compositions within a single segregation, with a subordinate volume of intermediate compositions trending to the composition of the host body itself. The segregations are most always of a characteristic chemical composition, which of course is set by the composition of the host body itself. And because they are relatively siliceous, even at the host liquidus temperature, they are significantly more viscous than the host magma and are thus physically, though not chemically, immiscible. Should the whole body later be remelted, homogenization by any normal means of convective stirring as in repeated transport is unlikely. These segregations thus represent a type of "siliceous noise" that, in effect, irreversibly appears in the basaltic system (Marsh, 1996). Through cycles of formation during solidification and accumulation during remelting, these segregations may contribute substantially to efficient chemical differentiation. It is these features that make the formation of silicic segregations in basaltic sills important to understand. This understanding may well reveal how many magmatic systems differentiate (Gunnarsson et al., 1998).

After introducing the concept of solidification fronts and reviewing the ideas advanced to explain the formation of silicic segregations, the general occurrence and basic chemical characteristics of silicic segregations are described. A general model of the chemical evolution of a typical body shows that silicic segregations form well within the upper solidification front from residual melt after ~60 to 70% (vol.) solidification. By use of this result and the fact that the segregations coarsen downward from sharp upper contacts, a physical model of segregation formation is next developed involving drawing in of local interstitial melt during sagging and internal tearing of the upper solidification front. This process is called here solidification front instability, or SFI. The physical details of the overall process are then discussed with an overview of the broader implications of SFI for magmatic differentiation in general.

2. SILL SOLIDIFICATION AND SOLIDIFICATION FRONTS

2.1. Sill Solidification

It is clear from the final distribution of phenocrysts in basaltic sills and lava lakes (e.g., Marsh, 1988), the horizon of juncture of the upper and lower cooling joint sets (e.g., Moore and Evans, 1967), and the direct drilling of Hawaiian lava lakes (e.g., Wright and Okamura, 1977) that sheetlike bodies of basaltic magma near and on Earth's surface cool and solidify more or less symmetrically (Mangan and Marsh, 1992). Sills as thick as 650 to 700 m (Mangan et al., 1993) and lava lakes as thick as 100 m (e.g., Helz and Thornber, 1987) show this characteristic. There are, however, some notable variations on this basic theme.

Magmas emplaced carrying large amounts of phenocrysts (e.g., Shonkin Sag Laccolith; Hurlbut, 1939) drop these crystals soon after emplacement and form thick piles of basal cumulates that expedite basal solidification. And some lava flows, such as that described by Long and Wood (1986), because of unusual surface conditions, may solidify strongly from the top down. Symmetry in sill solidification is also enhanced by similarity in the upper and lower wall rock thermal conditions. That is, because sills actually split the crust upon emplacement, the upper and lower contact temperatures are exactly the same at the onset of cooling. And because the sill is so much hotter than the wall rock itself, heat flows equally well upward and downward; the upper and lower thermal gradients are effectively identical. At later stages of cooling, when the magma is no longer dynamically viable, hydrothermal fluid flow may become effective in enhancing cooling in the upper crust (e.g., Carrigan, 1986). Hydrothermal fluids may become trapped beneath the sill, allowing late stage, subsolidus cooling to be more effective from the top. In this respect, it is important to emphasize that the amount of cooling necessary to bring the magma to the point of 50% crystallization is only ~100°C. Beyond this point, which is discussed more fully later, the magma is fully congested with crystals and any relative motion between liquid and crystals is extremely difficult. Relative to the total time necessary for the sill to reach near ambient crustal temperatures, the time to reach congestion is very short (Peck et al., 1977).

The rate of solidification, almost regardless of the convective nature of the inner region of magma, is that of a melt possessing latent heat, cooling and solidifying purely as a result of conductive heat transfer. Cooling follows conduction mainly because of the establishment of upper and lower solidification fronts in which any significant fluid motion, as a result of high viscosity, is doubtful and also because magmas posses no

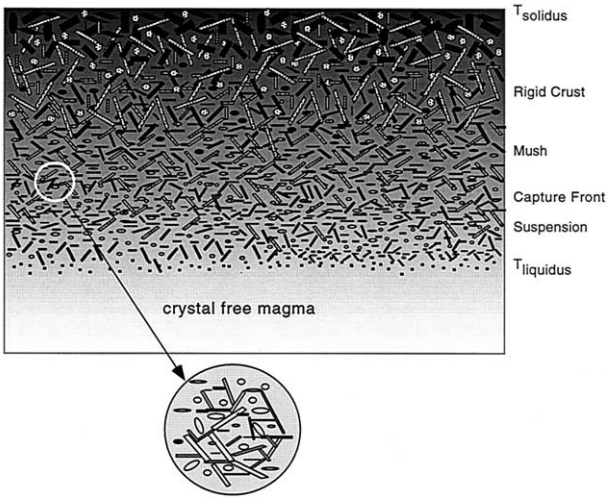

Fig. 1. Upper solidification front. The outer margin (top) of the front is defined by the solidus, and the leading or inner edge is the liquidus. The overall thickness of the front depends on the thermal regime, especially the age of the front and the temperature of the roof rock. The inset depicts the frameworklike structure of the crystals at ~30% crystals.

superheat (Marsh, 1989a,b; Hort et al., 1999). Conductive cooling is further encouraged in sills because of the insulating nature of the wall rock (Carrigan, 1988).

2.2. Solidification Fronts

The spatial relation between the liquidus and solidus defines a solidification front about any magmatic body (Fig. 1). In traversing this region, the magma goes from fully liquid to fully solid. With cooling, this bundle of isotherms propagates inward everywhere around the body, meeting in the interior at the point of final solidification. Although thin and sharp just after emplacement, the solidification front with time thickens in proportion to the square root of time, as is well known, for example, from the drilling of Hawaiian lava lakes (e.g., Wright and Okamura, 1977). In the ideal magma emplaced free of crystals, crystals nucleate and begin growing at the inwardly advancing liquidus. The viscosity there is essentially that of the crystal-free magma, and only when the crystallinity increases to ~25% does the viscosity increase by a factor of ~10 (Shaw, 1969; Ryerson et al., 1988).

At the trailing edge of the solidification front, near the solidus, the viscosity is enormous because the rock is nearly solid. Inward from this point, crystallinity decreases, but only when crystallinity decreases to ~50 to 55% does the viscosity begin to decrease dramatically as the magma makes the transition from a partially molten solid to a mushy liquid. This is the point of critical crystallinity marking the region of maximum packing of the solids where at all higher crystallinities the crystals form an interlocking network of some strength (Marsh, 1981). At lower crystallinities, the network of crystals is not fully interlocking (but see below), and the material behaves instead as a crystal-laden fluid possessing a large effective viscosity; the crystals (and vesicles) are unable to move freely relative to one another and the region behaves as a mush. This mushlike behavior continues inward with decreasing crystallinity (i.e., increasing temperature) until reaching the earlier-described region where the effective viscosity is within a factor of ~10 of the crystal-free magma viscosity. Within this innermost zone crystallinity (N) is low ($0 < N < 25\%$) and the sparse crystals are able to move freely relative to one another with little hindrance; the magma here is a suspension. These various rheological divisions can be summarized and classified as follows (Marsh, 1981, 1988, 1996).

1. Rigid crust. Bounded by the solidus ($N = 100\%$) and the point of critical crystallinity ($N = 50$ to 55%). This is the drillable portion of the solidification front commonly referred to as the "crust" in studies of Hawaiian lava lakes.
2. Mush zone. Bounded by the Capture Front ($N = 25\%$) and the region of critical crystallinity at maximum packing of the solids where $N = 50$ to 55%; crystal migration is difficult because of mutual hindrance.
3. Capture Front. The boundary marking the outer edge of the suspension zone outward of which settling crystals are unlikely ever to escape the solidification front
4. Suspension zone. Beginning at the liquidus, $N = 0$, and ending at the Capture Front at a crystallinity of about $N = 25\%$; small, sparse crystals can move freely relative to one another; and across this zone the effective viscosity increases by a factor of ~10.

Two aspects of this subdivided solidification front are important to emphasize. First, these are generalized definitions and are closely tied to the specific phase equilibria of the magma under study; the defining crystallinities will vary somewhat with magma type. In plagioclase-rich basalts, for example, an interlocking network of significant strength may form at crystallinities as low as ~30% (Philpotts et al., 1996). Second, the entire solidification front, which is always present, is a dynamic feature of solidification; the front propagates inward at an ever-decreasing rate and thickens with time. Because it is a dynamic feature, the solidification front initiates and competes with all physical and chemical processes occurring within its boundaries. We shall see later that the formation of silicic segregations is an integral reflection of solidification front propagation.

Within this framework of inward propagating solidification fronts, the spectrum of ideas concerning the origin and formation of silicic segregations can be discussed.

> We may now return to the commonly observed association of diabase and its salic differentiate. . . During the period when the magma has largely crystallized, "the straining-off or squeezing-out of the residual fluid magma" [A. Harker, 1909] is the most important process. —N. L. Bowen, 1915

3. ORIGIN OF SEGREGATION MELT

In any magmatic body the differentiated melt resides interstitially within the solidification fronts. Deeper within the fronts (i.e., closer to the solidus), this melt becomes increasingly more fractionated. The variation in the silica content of this melt as a function of crystallinity for a quartz tholeiite bulk composition, for example, is shown in Figure 2 as calculated by MELTS software (e.g., Ghiorso and Carmichael, 1987). (Also shown for later discussion are the variations in melt viscosity

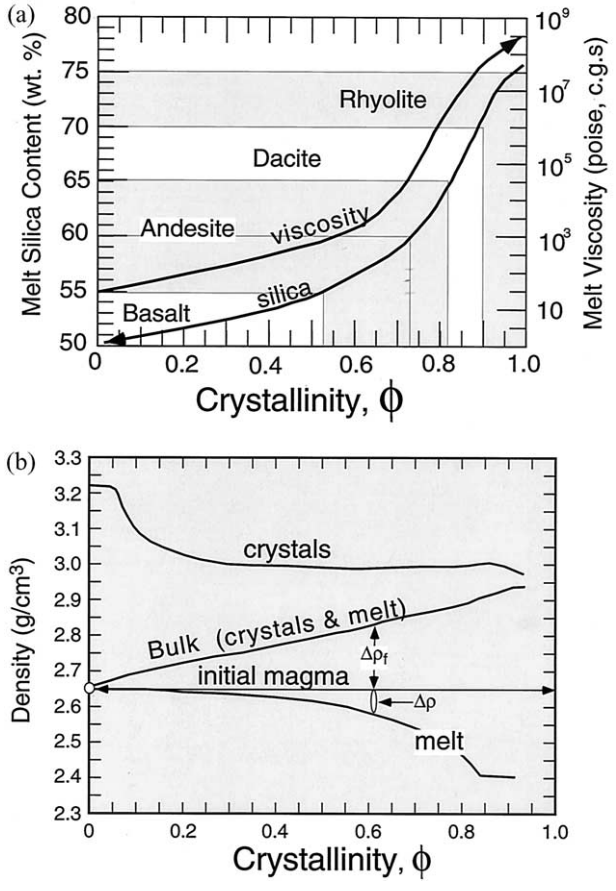

Fig. 2. (a) Change in melt silica content and viscosity with increasing solidification or crystallinity as calculated for a magma of tholeiitic composition by MELTS. (b) Variation in density with crystallinity for the solids, melt, and bulk system for the same tholeiitic composition as in (a).

and various densities.) As long known, serious enrichment in silica begins after ~50% crystallization, which is already relatively deep within the solidification front and is beyond the point when a rigid plagioclase network has formed. Strongly fractionated interstitial melts exist only after ~75% crystallization where the matrix is very strong, as will later be discussed in some detail, and melt extraction or emplacement can only occur by fracturing or porous media flow. Most silicic segregations have bulk compositions 5 to 10% richer in silica that the host basalt, which represents ~50 to 70% crystallization. Although using only silica as an indicator of degree of crystallization is clearly only approximate, a more detailed analysis of this fractionation process that uses major and trace elements reinforces this basic result (Zavala and Marsh, 2000, 2001). It is thus clear that the melt filling silicic segregations comes from this region of the solidification front, near 50 to 70% crystallization. But additional information on segregation location and texture is needed to determine whether the melt comes diapirically from the lower front or is segregated locally in the upper front.

In noting that silicic segregations in Antarctic sills cannot represent final residual or sandwich zone liquids because they occur at many horizons, Gunn (1966) suggested that late stage melt begins percolating upward once the whole sill becomes 80% crystalline (Fig. 3). The upward percolating melt forms lenses at successively deeper levels as the horizon of high strength rock migrates progressively deeper with cooling. At large degrees of crystallinity, however, melt migration is only possible if compaction takes place somewhere deeper in the underlying column, which is very unlikely at high crystallinity (see later). And melt cannot ascend to higher levels unless room is made for it through holes opening or removal of the resident melt. Philpotts et al. (1996) have, however, documented a clear case of a similar process in a diabase sill. Compaction in the innermost region of the lower front at low crystallinity allows buoyant melt to escape upward and enter the upper front. The process takes place at relatively low degrees of crystallization (~30%) and the segregated melt is not enriched in silica. A broadly similar process was suggested by Puffer and Horter (1993) to explain compositionally similar (i.e., nonsilicic) segregations.

This process is possible once the interstitial liquid in the upward moving lower solidification front (Fig. 2) becomes buoyant enough, perhaps with the help of vesiculation, to migrate upward and be replaced by denser overlying melt, (Goff, 1996; Caroff et al., 1997). This is a gravitational instability and the rising melt forms small plumes or diapirs (e.g., Marsh, 1988) that rise and lodge in the upper solidification front (Helz, 1980). Later drilling in Kilauea Iki Lava Lake convinced Helz et al. (1989) that such diapirs do in fact operate, but they do not directly form silicic segregations in the upper solidification front. They instead add slightly differentiated melt to a thermal horizon in the upper front equivalent to the source horizon in the lower front of the diapirs themselves. They cannot penetrate the upper front to any large extent because the upper front becomes increasingly strong upward and the resident interstitial melt itself is more buoyant than the invading melt. Nonsilicic segregations, therefore, may represent diapirs of interstitial melt from the leading region of the lower solidification front.

That silicic segregations are produced locally through tearing of the upper front is suggested by several observations (Fig. 3). First, in the well-exposed segregations of the Ferrar dolerites of Antarctica, the upper contact of the segregation is knife sharp, suggesting a sudden opening and not a pervasive interstitial inflow. Second, the coarsest crystals are along the upper edge of silicic segregations (Gunn, 1966; Wheelock and Marsh, 1993; Marsh, 1996; Zavala and Marsh, 2001). Apparently as the opening forms, the uppermost melt, being multiply saturated and close to thermal and chemical equilibrium, produces crystals able to enjoy uninhibited growth. Deeper in the segregations, the later arriving melt comes from greater depths in the front, is slightly hotter, and, in cooling to the ambient wall rock temperature, nucleates and grows progressively smaller crystals. The segregation texture is thus coarsest at the top and grades smaller downward until it meshes smoothly with the normal diabase texture. Third, the overall form of the segregations is fracturelike. Although commonly horizontal, they also sometimes climb and descend, showing clear crosscutting relations. In some areas of the Antarctic Basement sill a series of interconnected fracturelike segregations formed over a 5- to 10-m vertical section, forming a belt of segregations continuing horizontally for 50 to 100 m. Last, in drilling Kilauea Iki Lava

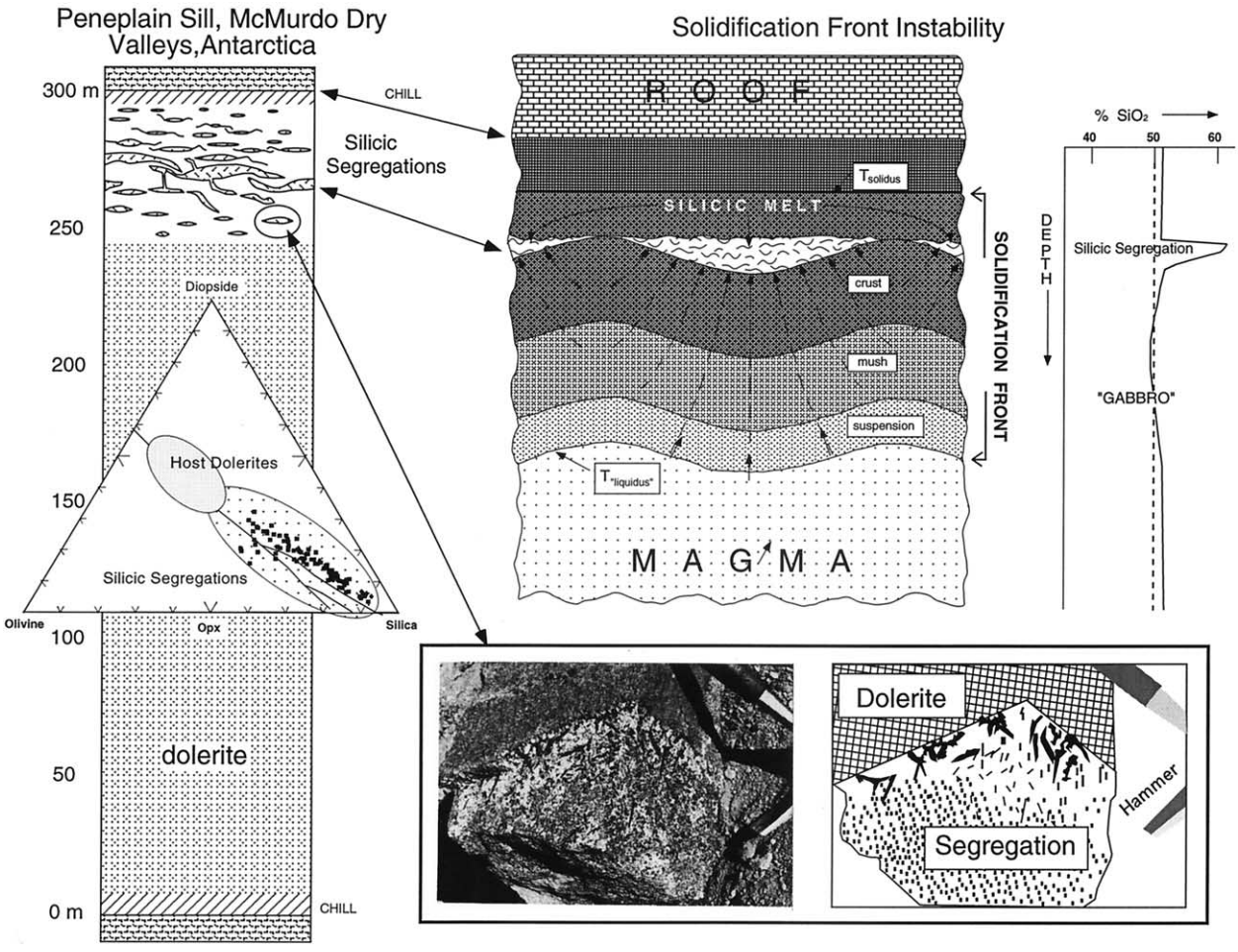

Fig. 3. (Left) Schematic depiction of the location, style, and context of silicic segregations in the Peneplain Sill, Antarctica. Superimposed on the sill section is the basalt normative ternary that shows the strong enrichment in silica of Antarctic silicic segregations relative to the host Ferrar dolerites. (Middle) Schematic representation of the general process of SFI, with the variation in silica content (right) that might be expected through a silicic segregation and its host rock. At the base is a photograph of the upper part of a typical segregation in the Basement Sill, Antarctica, accompanied by a sketch of the same segregation. Hammer placed for scale.

Lake, Helz and Thornber (1987) found temperatures to be 5 to 10°C hotter near segregations, based on bulk composition. If these melts were from the low crystallinity region of either the lower or upper front, the melt composition would record a much higher temperature.

It seems clear that silicic segregations form locally at crystallinities of 55 to 70% through tearing of the upper solidification front.

4. IDEAS ON SEGREGATION FORMATION

A few authors have considered segregations to be the vestiges of assimilation of wall rock or heterogeneity in the original magma (e.g., Bowen, 1910; Walker and Poldervaart, 1949), which may be so for some bodies. But it is clear from the long, undulating, fracturelike form, sometimes crosscutting nature, and textures of segregations that fracturing and filling with residual melt is the most likely mechanism of formation. The factors precipitating tension and fracturing in the upper solidification front are the principal physical questions explored here.

4.1. Tension in the Upper Solidification Front

For Makaopuhi lava lake, Wright and Okamura (1977) suggest that the upper crust becomes partially supported by the wall rock to the extent that, with progressive solidification and shrinkage, the underlying mush and melt periodically recede from the arching roof. This induces fracturing in the overlying much more rigid part of the solidification front. Although clearly possible in the smaller lava lakes, in thick, expansive sills, the roof must at all times effectively float on the magma, with no support from the sidewalls. The general idea of downward tension developing in the upper solidification front leading to horizontal tearing, however, is clearly of general importance. Another way to initiate vertical tension is through failure or slumping of the lower, mobile part of the upper solidification front. “The possibility arises that this zone periodically becomes too wide and too tenuous to support its own weight, causing subhorizontal tears to open up just above the base of the crust” (Helz, 1980). Helz further reasoned that the underlying melt might be of low enough density, especially if con-

taining some vesicles, to migrate upward and fill the tears. Because the melt may possess yield strength and thus resist flow, Helz thought this mechanism unlikely to be generally applicable to Kilauea Iki lava lake, where segregation veins are common. Even the melt alone, neglecting the crystals, underlying the fracture horizon is, as will later be shown, only very slightly less dense than the still deeper uncrystallized magma, and is thus unlikely to rise simply by buoyancy to fill the fractures.

4.2. Local Gas Buildup

The local buildup of vesicles due to progressive crystallization, especially in lavas and lava lakes, may produce a local overpressure, which promotes fracturing in the solidification front and filling by local residual (e.g., Sonnenthal, 1990). Because the gas produces a local overpressure, however, the melt might instead be driven away from the tear unless the tear first fills with gas that eventually leaks away through tiny ephemeral vertical cracks and is replaced by local melt. This mechanism for the production of segregations filling vesicles has been documented and modeled by Anderson et al. (1984). This process operates best at very high crystallinity where active inward propagating fractures can access large vesicles in contact with interstitial melt. Although this could be a secondary contributing factor, it seems difficult to produce thick ($\sim$0.5 m) silicic segregations at significant depths in active solidification fronts principally by this process.

4.3. Gravitational Instability

Because the distance between the inward propagating liquidus and solidus increases systematically during solidification, the effective weight of the solidification front increases greatly with time. Eventually this downward stress may exceed the local strength of the partially molten rock causing fracturing, which upon continued sagging simultaneously draws local, interstitial melt into the fracture (Marsh, 1991, 1996; see also Sonnenthal, 1990, and personal communication). Although somewhat similar to Helz's mechanism, here the solidification front begins to de-laminate or tear away from the more fully crystallized stronger overlying rock, producing isolated segregations in smaller bodies. Melt flow into the tear occurs mainly in response to the anomalous pressure gradient caused by the sinking, porous plungerlike lower solidification front. In sufficiently thick solidification fronts, the front may wholly detach, entirely freeing the earlier formed segregations to collect into significant batches of late stage melt.

5. PHYSICS OF SEGREGATION FORMATION

Because of cooling and crystallization, both the upper and lower solidification fronts are as a whole denser than the uncrystallized magma of the core region. This may cause the lower front to undergo compaction, if it becomes thick enough, but it is basically stable to other deformation. The upper or roof ward front, however, is inherently gravitationally unstable (Fig. 3). As it thickens with cooling, gravity exerts an ever-increasing downward directed stress or tension on the solidifying magma and the roof rock. The front wants to settle, and is stabilized only by the strength of the growing matrix of solids. It will tear open at a horizon where the stress overcomes this local strength.

As long as the crystals of the front are interconnected, the front has strength. This strength depends critically on the extent of connectedness of the growing crystals. At greater than $\sim$50% crystals, the crystals form a network regardless of the exact type of crystals (Marsh, 1981). But in magmas where plagioclase is a dominant phase, which is generally true for rocks containing silicic segregations, this framework may continue downward to crystallinities as low as 25 to 30% (Philpotts and Carroll, 1996). As crystallinity decreases downward in the front, strength also diminishes rapidly downward through the rigid crust and mush zones until the matrix becomes an ensemble of tiny disconnected minerals at the suspension zone. The residual liquid in the front is buoyant and it is only the crystals that generally make this overall unit heavy (Fig. 2). Because the segregations form where the crystallinity is in the range of 60 to 70%, the segregations clearly develop in or near the transition between the rigid crust, where the magma has significant strength, and the mush zone, where the magma has much less strength. The variation in strength is surely continuous, and the fracture occurs at a weak link in the front.

The critical condition for stability is that the strength of the crystal network must increase upward fast enough to support the increasing weight of the solidification front. That is, the mass of solids or modal mineralogy forming the interconnected network must increase upward sufficiently fast to maintain the local strength at a level beyond that necessary to support the downward directed gravitational loading. This situation is directly analogous to the downward increase in cross-sectional area of a tall, solid column or pillar necessary to offset the internal stress due to the weight of the overlying column itself (e.g., Timoshenko, 1940). That this condition for magma might never be generally satisfied comes from the recognition that the local modal mineralogy, and thus the local strength, is controlled by phase equilibria, which has no inherent analytical connection to the required strength of this assemblage. Strength comes from building a structural network using any given modal mineralogy, but this strength may not be sufficient to sustain the structural integrity of the meshwork. We shall see that the geometric forms of the functions describing the variations in crystallinity dictated by these two conditions (i.e., strength vs. phase equilibria) are at odds to one another. So, provided the basic condition of density contrast is met, the front is inherently unstable.

The inherent gravitational instability of the upper solidification front is modulated or regulated by the rate of advancement of the high strength rigid crust relative to the rate of the tearing instability, which itself is regulated by the rate that local interstitial melt fills the tear. The fractures can open no more rapidly than the rate at which melt can enter and fill the fracture. If this opening-infilling process is slow relative to the rate of solidification, segregations cannot form. Moreover, because it is relatively easy for melt immediately adjacent to the fracture to inflow, small stringerlike segregations will form early. But as the rates of cooling and solidification slow and the solidification front thickens, instability is increasingly successful. At greater depths from the roof, increasingly thick segregations form. Near the center of the body with approach of the lower

Table 1. Symbols.

Greek	
$\Delta\rho$	Density contrast
$\Delta\rho^*$	Sum of $\overline{\Delta\rho_f}$ and $\overline{\Delta\rho}$, where the overbars denote mean quantities
$\Delta\rho_f$	Density contrast driving the falling solidification front
δ	Thickness of the region immediately below segregation controlling flow of interstitial melt
δ_s	Thickness of the region supplying melt filling the segregation
δ_o	Crystal fraction at beginning of crystalline network
ϕ	Crystal fraction
μ	Viscosity (shear) of melt, subscripts; *m*, maximum; *o*, initial value at ϕ_o
σ_f	Strength of front at $\phi = 1$
σ_o	Strength of front at ϕ_o
Roman	
b	Latent heat parameter
C_p	Specific heat
$d(t)$	Thickness of the unstable part of the solidification front
e	Porosity $(1 - \phi)$
g	Gravity
H	Latent heat
h	Full thickness of solidification front
h_L	Position of liquidus from upper contact
h_S	Position of solidus from upper contact
K	Thermal diffusivity, subscripts: 1, solidus; 2, liquidus
K_D	Permeability, subscripts: *m*, minimum; *o*, initial (maximum) value at ϕ_o
L	Thickness of the sill
N	Crystallinity (%)
P	Pressure
S	Thickness of the segregation
t	Time
T_o	Initial temperature of magma
T_w	Initial temperature of wall rock
V_m	Darcy melt velocity
V_p	Velocity of melt in pores of solid matrix
V_s	Velocity of solid matrix
z	Upward distance from ϕ_o
z_o	Thickness of SF that has strength ($\sim 0.25 < \phi < 1.0$)
z_p	$= z/z_o$ nondimensional distance upward from ϕ_o, $(0 < z_p < 1)$

solidification front the rate of isotherm advancement increases and segregation formation ceases.

Some formalism is next developed to describe the upward increase in crystallinity necessary to sustain the strength of the front under increasing gravitational stress due to thickening of the front. This result will then be compared with the upward variation in crystallinity predicted by phase equilibria. Next, equations will be given to describe the rate of cooling and growth of the upper solidification front, the variation in tensile strength and permeability with depth, the downward tension due to the growing upper solidification front, and the rate of flow of the interstitial melt. These results will allow the basic process of instability to be examined.

5.1. Crystallinity Variation Necessary to Sustain Strength

To sustain strength with increasing thickness or net weight of the front hanging from the roof, the local increase in crystallinity ($d\phi$) must add enough strength to offset the net increase in weight ($\phi\Delta\rho g dz$) of each dz thickness of the front (Table 1 summarizes the symbols used in this discussion). If the strength of the fully crystalline rock is σ_c, then

$$\sigma_c d\phi = \phi\Delta\rho g dz \tag{1}$$

or

$$\frac{d\phi}{\phi} = \frac{\Delta\rho g}{\sigma_c}\, dz, \tag{2}$$

which, upon integrating, becomes

$$\phi = \phi_o \exp((\Delta\rho g/\sigma_c) z) \tag{3}$$

The quantity ϕ_o represents the initial crystallinity at the start of the interconnected network, which, judging from the results of Philpotts and Carroll (1996) in magmas of broadly tholeiitic basaltic composition, is formed by plagioclase at $\phi \sim 0.25$ to 0.30. The density contrast, $\Delta\rho$, is $\sim$0.1 g/cm^3, and g is gravity. Although the strength σ_c is unknown, it is clear that for stability crystallinity must increase exponentially upward in the crystalline network.

Variations in crystallinity with nondimensional height ($z_p = z/z_o$, where z_o is front thickness) for fronts of thicknesses (i.e., $0.25 < \phi < 1$) of 10, 50, 100, 150, and 200 m and for a characteristic strength of $\sigma_c = 0.05$ bars are shown by Figure 4a and similarly by Fig. 4b for a 10-m-thick front for a range of strengths from 0.015 to 0.15 bars. Also depicted in these figures is the variation in crystallinity predicted from phase equilibria as calculated by MELTS, as mentioned earlier when introducing Figure 2. For thin, strong fronts, crystallinity need only increase slowly upward to stabilize against tearing. But for thick or weak fronts, crystallinity must increase unreasonably fast with height to prevent instability.

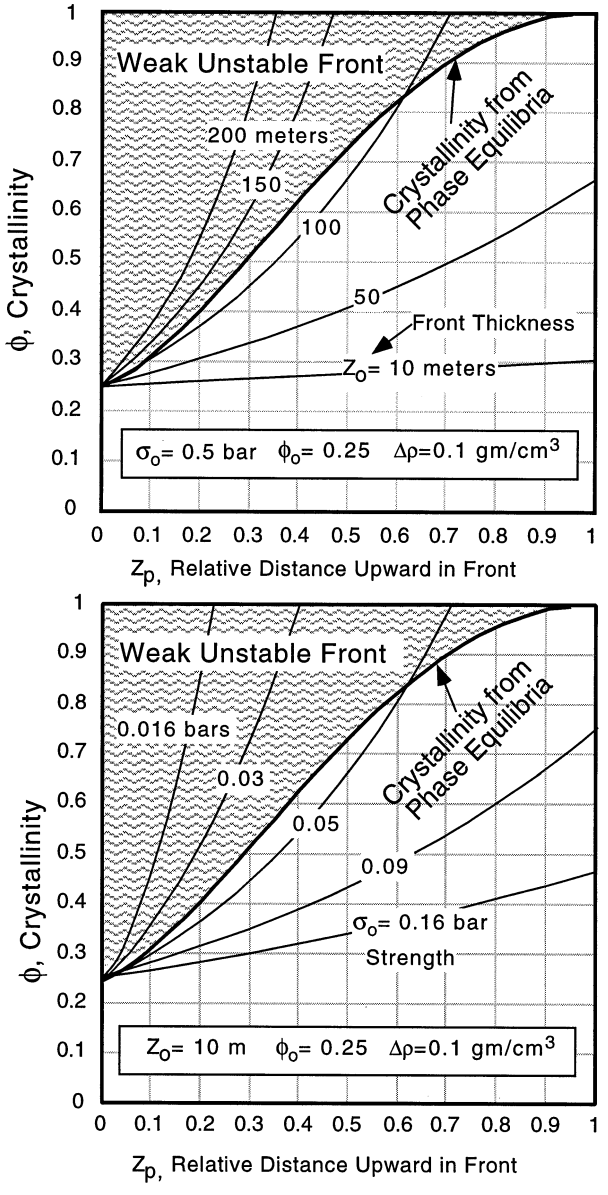

Fig. 4. Variation in crystallinity necessary to prevent tearing in comparison with the increase in crystallinity due to solidification as determined from phase equilibria. The upper curves show the effect of front thickness for constant strength, and the lower curves show the effect of strength changes for a front 10 m thick. The region in each where the front is weak and unstable to tearing is indicated.

The calculated variations in melt viscosity and silica content with increasing crystallinity during solidification are shown by Figure 2. To anticipate later needs, also shown here are the bulk and liquid phase densities through the crystallization interval. The buildup of crystals during cooling is broadly similar for many basaltic-andesitic bulk compositions. Liquid density decreases and the bulk density increases with solidification. Overall, the front becomes heavy and the melt becomes light; it is this contrast in density that promotes instability of the solidification front. Not all magma compositions have these characteristics; some liquids harbor iron until late and thus become relatively dense and seek to drain from the front. Nevertheless,

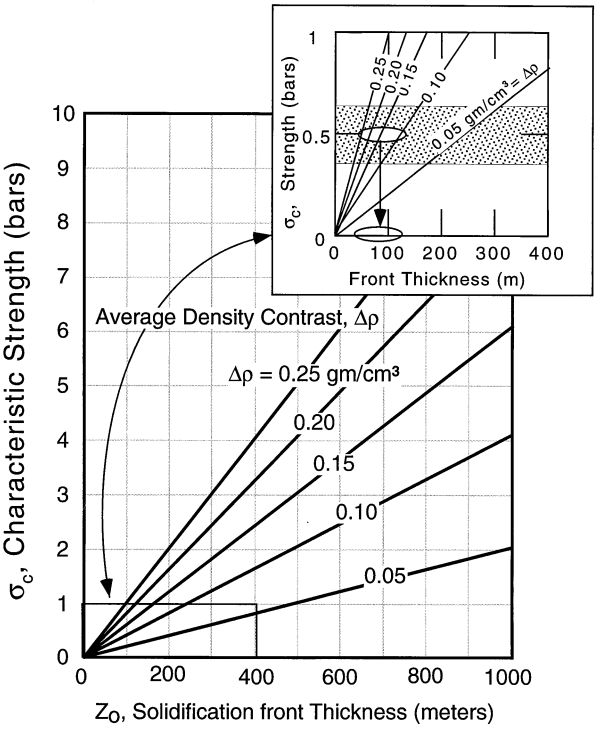

Fig. 5. Strength necessary at 65% crystals to prevent or to allow a tear to develop for a given thickness (Z_o) of solidification front and for a range of density contrasts. Clearly, for a given strength, the heavier the front, the thinner it will be and the more prone to instability and tearing.

the critical issue for the moment is that the actual strengthening of the front due to increased solids is dictated by phase equilibria, which does not necessarily follow that required, on purely structural grounds, to prevent tearing. That is, the separate variations in crystallinity from phase equilibria and structural considerations are not generally coincident but cross somewhere in the crystallization interval, which defines the point of instability. This point is known independently, as mentioned earlier, from chemistry, to be at $\phi \sim 0.6$ to 0.7, which from Figure 4 puts it at a nondimensional distance upward in the front of about $z_p \sim 0.4$.

The tradeoff in required local strength, total front thickness, and density contrast at this point of intersection is found from Eqn. 3.

$$\frac{(\Delta\rho g z_o)}{\sigma_c} = \frac{\ln(\phi/\phi_o)}{z_p}. \tag{4}$$

Substituting the values for the known parameters on the right (i.e., for example, $\phi \sim 0.65$, $\phi_o \sim 0.25$, and $z_p \sim 0.4$), gives

$$\sigma_c = \frac{\Delta\rho g z_o}{2.4}, \tag{5}$$

and this relation for a series of density contrasts is shown by Figure 5. The strength required at this specific horizon to prevent tearing ranges between ~1 and 10 bars (0.1 to 1 MPa) for fronts of thickness 100 to 1000 m. But because the physical nature of the front at any *relative* horizon within the front does

not depend on front thickness, the local strength is also independent of front thickness and is of some, as yet unknown, constant magnitude. That the front is observed to tear here means that these values set an upper bound for the strength of the front. The actual strength can only be found from a specific natural example and perhaps from experiments, which we next consider.

5.2. Tensile Strength of the Solidification Front

The only experimental estimate of the strength of hot basaltic rock is that of ~30 MPa (300 bars) at 700°C measured by M. P. Ryan and reported by Schultz (1993). This temperature is well below the solidus, but the volcanic rock sample may well have contained some glass and cannot thus be taken as a holocrystalline rock. At temperatures above the solidus, Shaw (1980) estimated the strength of mostly molten Hawaiian basalt from in situ viscosity measurements. At 25% crystals he estimated the strength to be $\sim 5 \times 10^{-6}$ MPa, at 30% crystals $\sim 3 \times 10^{-4}$ MPa, and at 50 to 60% crystals $\sim 10^{-2}$ MPa. This last estimate is based on the appearance of "melt-filled gash fractures," which are the same basic features under consideration here, and hence cannot be used as an estimate of strength independent of the process itself.

There is a significant difference in the estimates of strength between the values of Shaw (1980), which are in the melting range, and that of Ryan, which is at a subsolidus temperature. There are probably two good reasons for this contrast. First, as Schultz (1993) discusses, small "intact" samples of rock, free of cracks and other imperfections common to large rock masses, are much stronger, by a factor of ~100, than in situ rock masses. Second, the presence of melt-filled pores does not greatly weaken rock until the melt is so abundant that the solid structure of the rock itself breaks down (Sleep, 1988). Taken together, the strength of partially molten basalt at low melt fractions (i.e., $<$ ~30 to 40%) is probably ~1 bar (0.10 MPa). And near the point of critical crystallinity where the solid structure breaks down as the rock becomes a viscous mass, the strength decreases greatly to the range estimated by Shaw (1980) (i.e., $<$ $\sim 10^{-4}$ MPa). That this last limit is meaningful can be seen by noting that a 1-cm cube of basalt at ~25% solids deforms very slightly under its own weight (Philpotts, personal communication), which represents a strength of $\sim 10^{-3}$ bar (10^{-4} MPa). These estimates of strength through the solidification front are shown schematically by Fig. 6, which suggests a convenient, albeit certainly only approximate, analytical representation of strength (σ_s)

$$\sigma_s = \sigma_o \left[\frac{\sigma_f}{\sigma_o} \right]^{((\phi - \phi_o)/(1-\phi_o))} \tag{6}$$

where σ_o ($= 10^{-3}$ bars) is the strength at ϕ_o and σ_f ($=$ ~300 bars) is the strength at the solidus where $\phi = 1$. This variation is also shown by Fig. 6. The strength near $\phi \sim 0.65$ is ~0.5 bars (0.05 MPa), with a likely uncertainty of at least 50%. It should be understood that it is unlikely that strength varies smoothly through the front, but rather varies in response to the detailed structural development of the crystalline meshwork (Marsh, 1996). These are also maximum estimates for failure under tension, the strength for which is characteristically an

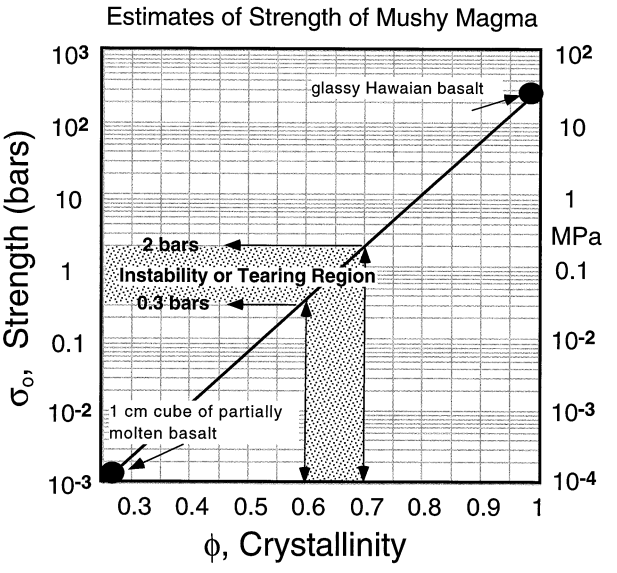

Fig. 6. Estimates of the strength of partially molten rock through the crystallization interval. The three regions where something is known of the strength are indicated; the log-linear line through the diagram is largely hypothetical.

order of magnitude lower than that for shear or compressional failure (e.g., Jaeger and Cook, 1979). Nevertheless, using this value (0.5 bars at $\phi \sim 0.65$) with the results of Figure 5 (inset), most fronts will begin tearing once they are ~50 to 100 m thick almost regardless of the density contrast. Thicker fronts will fail repeatedly, and may, if the sheet of magma is thick enough, fall free of the remaining solidification front.

These overall estimates of strength in basaltic magma are also broadly consistent with experimental results on granitic rocks (e.g., Arzi, 1978; van der Molen and Paterson, 1979), which results were originally considered by Marsh (1981) during development of the concept of solidification front rheology, dilatancy, and critical crystallinity. These experimental results are of limited usefulness, however, because they are at strain rates that are enormously larger ($\sim 10^{-4}$ s^{-1}) than the strain rates characteristic of the present process ($\sim 10^{-10}$ s^{-1}), which can be estimated from the results below. At large rates of strain during shear deformation, the rate of deformation may be regulated by the rate of melt flow into areas experiencing dilation. In granitic systems, the large viscosity of the melt coupled with large strain rates makes this an important process as discussed by Renner et al. (2000).

These estimates of strength (i.e., Fig. 6) and the conditions for failure are clearly met in many sills. It is thus of interest next to investigate if bounds can be placed on the rates of tear opening, which are largely controlled by the rates of local cooling or solidification.

5.3. Cooling Rate of a Sill

The cooling of a deeply buried sheet has been largely understood ever since the early studies by Lane (1898) relating cooling rate to grain size in diabase dikes. Later J. C. Jaeger gave many insightful and valuable analytical contributions

(e.g., Jaeger, 1968) on the cooling of dikes and sills. The central difficulty in the analytical description of sheet cooling is the inherent nonlinearity introduced by the evolution of latent heat during solidification. Analytical results are possible under certain conditions (see, e.g., Carslaw and Jaeger, 1959) and Jaeger (1957) shows how special solutions with latent heat evolution at a specific temperature can be adapted to include the effect of crystallization over a range of temperatures through use of an increased specific heat. A versatile numerical method is also available due to Delaney (1988; see also Ghiorso, 1991). Here we are interested in the basic physical interactions of the process, and it is both particularly revealing and convenient to use an analytical approach. We thus assume, to begin with, for simplicity and to introduce the basic method of analysis, conductive cooling without latent heat; the effect of latent heat is to slow cooling and crystallization, which can be easily evaluated later.

The velocity of advancement of any particular isotherm within a sill (i.e., an infinite horizontal sheet) is found by considering the total derivative of temperature in the conductively cooling body.

$$dT' = \left(\frac{\partial T'}{\partial t'}\right) dt' + \left(\frac{\partial T'}{\partial x'}\right) dx'. \tag{7}$$

Here, T is temperature, x is distance into the body, and t is time; the primes on each variable denote nondimensional quantities, which will be explicitly described below. Because for any isotherm T = constant or $dT = 0$, rearranging gives

$$\left.\frac{dx'}{dt'}\right|_T = -\left(\frac{\partial T'/\partial t'}{\partial T'/\partial x'}\right). \tag{8}$$

This describes the (nondimensional) rate of advancement or velocity of an isotherm in the course of cooling of the body. That is,

$$V'_T = -\left(\frac{\partial T'/\partial t'}{\partial T'/\partial x'}\right), \tag{9}$$

where t' and x' are, respectively, nondimensional time ($t' = Kt/L^2$) and distance ($x' = x/L$), L is the half thickness of the sill, K is thermal diffusivity, and t is time. The nondimensional velocity (V') is thus related to the dimensional velocity (V) by $V' = (L/K)V$.

Eqn. 9 is general and to obtain specific results the well known solution can be employed for conductive cooling of a deeply buried sheet of half thickness L. (I hasten to add, however, that the following results do not depend critically on the exact depth of sheet burial, especially for sheets deeper than a depth $2L$.)

$$\frac{T - T_w}{T_o - T_w} = \frac{1}{2}\left[erf\frac{(1 + x')}{\sqrt{4t'}} + erf\left(\frac{1 - x}{\sqrt{4t'}}\right)\right], \tag{10}$$

where *erf* is Gauss's error function. The initial body temperature, which is taken to be uniform, is T_o and the initial wall rock temperature is T_w. Forming the derivatives necessary for Eqn. 9 gives, after substitution and some lengthy and tedious manipulation,

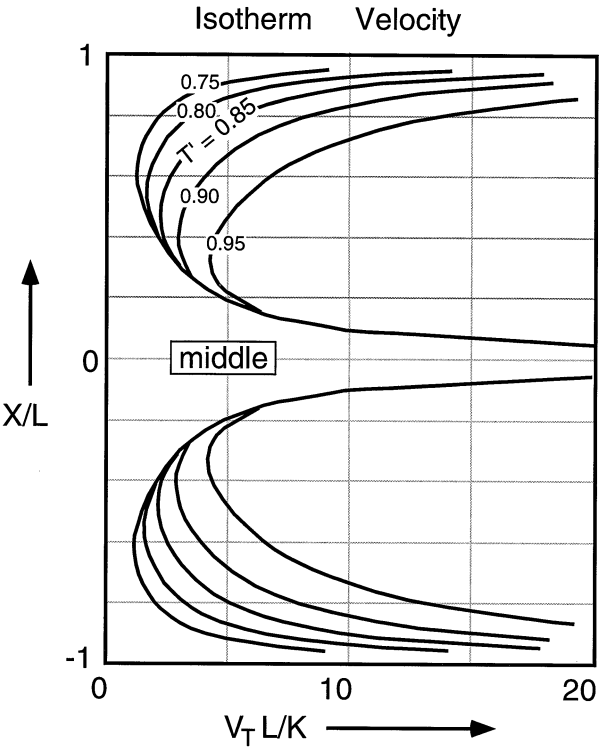

Fig. 7. Velocity of inward advancement of various isotherms as a function of distance $X'(= X/L)$ in a deeply buried sheetlike body.

$$V'_T = -\frac{1}{2t'}\left[x' - \coth(2x'/4t')\right], \tag{11}$$

which was first derived by Jaeger (1968) after having been deduced qualitatively by Tomkeieff (1940).

The propagation velocity found from this result for a number of isotherms is shown by Figure 7. This velocity is, understandably, large near the upper and lower contacts, but as noted by Jaeger it is, perhaps less understandably, also large at the center of the body. The large isotherm velocities at the center reflect the approach of both cooling fronts, taking ever more heat from an ever-decreasing volume of the sheet. This also indicates that the temperature field has a point of symmetry at the center, which makes the denominator in Eqn. 9 go through zero.

Concerning the present problem, segregation formation is favored by slow cooling, which is optimized in a region approximately midway between the sill center and top. The inclusion of more complicated cooling solutions involving latent heat will significantly affect the actual rates of isotherm advance (they will slow), but the pattern of isotherm advance is essentially a geometric effect and is unlikely to differ much from that shown by Figure 7. For a lava flow or lava lake, the symmetry of Figure 7 is lost as a result of more rapid cooling from the roof and thus the interior region of rapid isotherm advance occurs in the lower half of the body; the optimum region is thus widened.

Overall, velocities (nondimensional) on the order of two to five at the upper and lower midsections and >20 at the edges and center can be expected. These estimates are useful in determining how long it takes the front to move through any

specific horizon of the body. This time is strongly dependent on the thickness of the front, which increases markedly with time. We now turn to determining the variation in solidification front thickness with time.

5.4. Solidification Front Thickness

The thickness of the solidification front itself, which is the distance between the liquidus and solidus, is crucial to knowing the downward-directed tension due to the weight of the front and also the time of passage of the front at any specific horizon. This stress also drives the local residual melt into the opening fracture.

All solutions for the position of the inward moving liquidus and solidus (h_L and h_s, respectively) with or without latent heat and even including thermal convection in the core region of the sill, are of the forms

$$h_s(t) = 2b(K_1 t)^{1/2} \tag{12a}$$

$$h_L(t) = 4(K_2 t)^{1/2}, \tag{12b}$$

where K_1 and K_2 are, respectively, the thermal diffusivity of the solidus and liquidus assemblages, t is time, and the parameter b includes the effect of latent heat (Carslaw and Jaeger, 1959). From analytical solutions of cooling of a lava lake, for example, involving no latent heat, b = ~2; for latent heat evolved at a single melting temperature, b = ~0.75; and for latent heat evolution over, say, a 200°C range of crystallization, b = ~0.6 (e.g., Jaeger, 1957). Hawaiian lava lakes follow Eqn. 12a with b = ~0.8 (Turcotte and Schubert, 1982; Mangan and Marsh, 1992); and for deep burial of a melt sheet b is expected to be ~0.5, which we adopt henceforth along with a thermal diffusivity of $K_2 \sim K_1 = 10^{-2}$ cm^2/s. These can be easily changed in the ultimate formulation. The agreement between the analytical and observed results is generally close enough not to warrant concern.

The constant b is determined by a transcendental equation, which is usually solved graphically, but the solution also can be fit with a simple analytical function, which is particularly convenient. Thus, b is given by the approximate relation

$$b = \left(\frac{C_p(T_s - T_w)}{5H\sqrt{\pi}} \right)^{2/5}, \tag{13}$$

where C_p is specific heat, H is latent heat, and T_s is the solidus temperature. An interesting feature of this formula is the dependence of b on the contact or wall rock temperature (T_w). When T_w is equal to the solidus temperature T_s, $b = 0$, and the solidus does not propagate inward; only the liquidus moves inward, creating a wide solidification front until the center of the body begins to solidify whence the solidus begins also to move to the center. This must happen in the lower crust.

The local thickness of the solidification front is given by

$$h(t) = h_L(t) - h_s(t) \tag{14}$$

A full numerical solution of this solidification problem, including all the effects of latent heat distributed between the liquidus and solidus, shows this equation to be accurate (Zieg and Marsh, 2002).

As the solidification front thickens, the leading half or mush exerts a downward-directed tension on the much more rigid, cooler part of the solidification front due to its density contrast ($\Delta\rho$) with the underlying, uncrystallized magma. This tension amounts to

$$\sigma = (\Delta\rho)\, g h(t), \tag{15}$$

or, using 14 and 12,

$$\sigma = (\Delta\rho)\, g(4 - 2b)(Kt)^{1/2}, \tag{16}$$

and this is also the pressure driving the interstitial melt into the tear. The flow of melt through the porous matrix of crystals also depends on the local permeability and viscosity of the interstitial or residual melt. This flow is considered next.

5.5. Flow of Interstitial Melt

Because of the commonly observed sharp upper contacts and characteristic fineing downward of crystals in the segregations, as explained earlier, the inflowing melt must move upward through a matrix of approximately 25 to 70% solids. This extensive lattice begins near the solidus and continues downward, becoming increasingly fragile until a crystallinity of ~25% where it breaks down entirely. The strength of this lattice as already discussed decreases greatly downward and at some point is weak enough to deform as a viscous, particle-laden fluid. During instability the overall upward flow of interstitial melt carries free crystals upward, deeper into the interstices of the uppermost lattice or meshwork. This may eventually partially plug the lattice, stifling further flow, curtailing the instability. Understanding the melt flow through the porous lattice is central to understanding the instability itself, which can be done by Darcy's law.

Darcy's velocity is a measure of the fluid (i.e., melt) flux per unit area (V_m) (e.g., Phillips, 1991)

$$V_m = -\frac{K_D}{\mu}\left[\frac{\partial P}{\partial z} + \Delta\rho g \right], \tag{17}$$

where K_D is permeability, μ is melt viscosity, $\Delta\rho$ is the local density contrast between the melt and solids, and $\partial P/\partial x$ is the local vertical pressure gradient driving the flow, which decreases upward in the direction of flow, hence the sign. In a large open system where the solids can move *independently* of the melt, as in melt migration in the mantle, an additional term must be added to the above equation.

$$V_m = -\frac{K_D}{\mu}\left[\frac{\partial P}{\partial z} + \Delta\rho g \right] + (1 - \phi)V_s. \tag{18}$$

If there is no pressure gradient and no density contrast, there is no porous flow, and the only transport of the interstitial melt is by the motion of the matrix of solids containing the melt. That is,

$$V_m = (1 - \phi)V_s \tag{19}$$

In this example, the solids and melt can move independently, at least locally, of one another. This is in contrast to the present SFI situation where there is no motion of the solids independent of the melt. In fact, it is exactly the motion of the solids, in wanting to settle, that allows the interstitial melt to move at all.

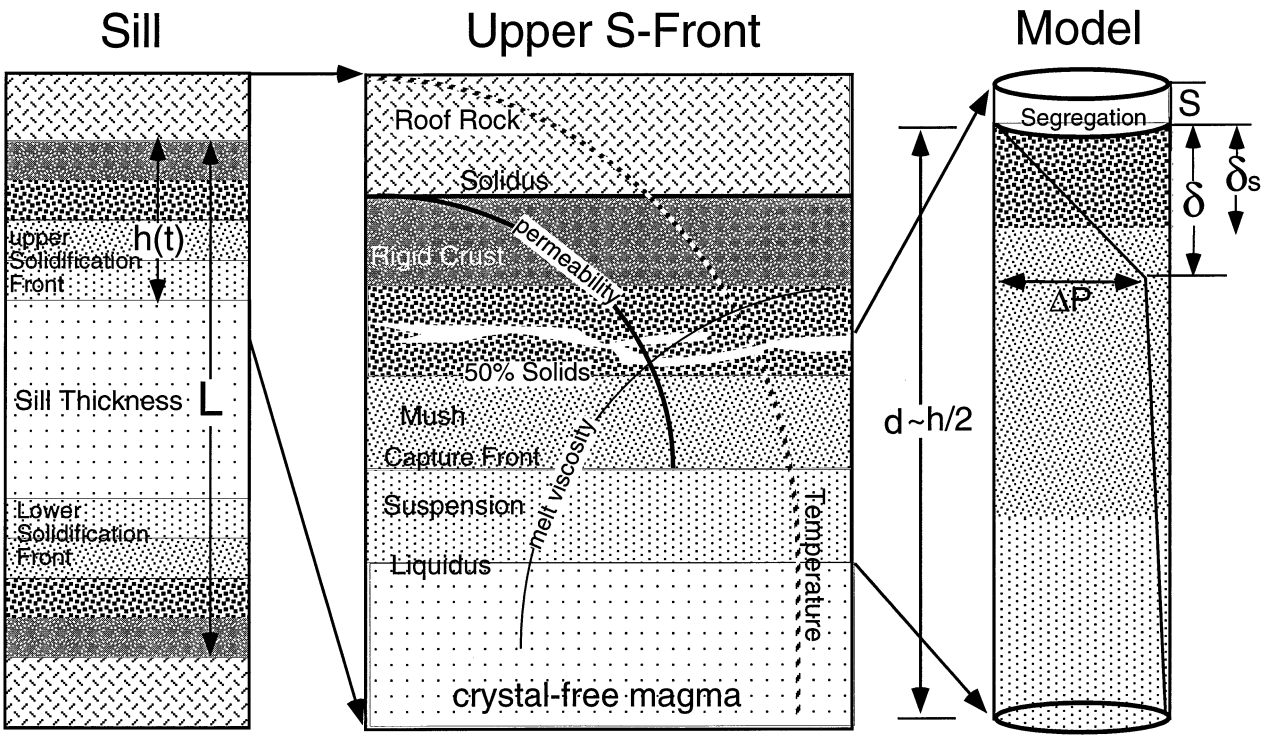

Fig. 8. Schematic representation of the sill solidification fronts, including the rheological divisions, and the length scales and physical property variations (melt viscosity and permeability) pertinent to the model of SFI.

Hence, for conservation of mass in this closed system, the upward flux of melt must equal the downward flux of solids (Q_s). Then for SFI,

$$V_m = Q_s = \phi V_s \tag{20}$$

which distinguishes this system over that exemplified by Earth's mantle.

If the solids do not move downward, the melt will not move upward. Moreover, the factor $(1 - \phi)$ measures the porosity or melt fraction, which relates the flow velocity in the pores (V_p) to the Darcy velocity (V_m).

$$V_m = (1 - \phi)V_p \tag{21}$$

It is thus clear that the rate-controlling step in melt migration, as described by Eqn. 17, is the resistance to flow through the matrix of crystals underlying the tear. This resistance regulates the rate of tearing of the front. Once V_m is known, V_s and V_p can be determined from, respectively, Eqns. 20 and 21, and the filling time for any given tear also can be determined. *The filling time must be sufficiently fast relative to the local rate of crystallization or the solid matrix will strengthen beyond that allowable for further instability.* Hence, the rate of melt migration is critical to the whole process.

The upward melt flow is driven both by a pressure gradient induced by sinking of the heavy solidification front and by the chemically produced low density or buoyancy of the interstitial melt. Each driving force exists independent of the other, which is distinct of usual flows in porous media where uneven density due to heating also produces the non hydrostatic pressure gradient. So, both driving forces stem from density contrasts. One is on a local or granular scale and one is on the scale of the front thickness itself. The local density contrast, judging from the results shown by Figure 4, is similar to that of the front itself. This latter density contrast ($\Delta\rho g$ in Eqn. 17) shows that, if a hole were to open in the front, the local melt would automatically move upward, even in the absence of the downward motion of the solids. It is, of course, not possible for a hole to appear spontaneously (except perhaps by the sudden escape of gas from a vesicle or cavity), and so this effect also operates in response to the tearing as a result of the moving solids. But the melt moves more easily than it would if this density contrast did not exist; it enhances the effect of the pressure gradient.

The overall pressure differential driving the flow is given by

$$\Delta \mathrm{P} = \Delta\rho_f g d(t), \tag{22}$$

where $d(t)$ is that part of the front that is unstable (Fig. 8), which is proportional to the full thickness ($h(t)$) of the solidification front. The subscript f denotes henceforth the density contrast driving the falling of the front, as described in Figure 2. Were this gradient exerted uniformly across the full thickness $d(t)$, $\partial \mathrm{P}/\partial z = \Delta\rho_f g$ and the melt velocity of Eqn. 17 becomes independent of the thickness of the lower part of the front. But because the permeability varies strongly in the front, flow resistance is concentrated in a relatively narrow region beginning at the base of the segregation itself (Fig. 8). That is, the upward flow velocity is approximately constant and the

local pressure gradient must vary in concert with changes in permeability (Phillips, 1991, p. 64).

The mean pressure gradient over this region is found from Eqn. 17

$$\frac{\partial \bar{P}}{\partial z} + \overline{\Delta \rho g} = -V_z \frac{1}{d} \int_0^d \frac{\mu(z)}{K_D(z)}\, dz, \tag{23}$$

where d, as above, is the unstable part of the solidification front marked at the top by the segregation and at the base by the point where the crystal lattice breaks down to a suspension. The accompanying effect of the local density contrast of the interstitial melt is also taken as a mean value over the region, but is not affected by the variations in permeability and viscosity. The effect of increasing viscosity of the melt as a result of increasing silica with increasing crystallinity is handled by including viscosity within the integral above. Convenient functions for the variations in permeability and viscosity are

$$K_D(z) = K_O \left[\frac{K_m}{K_o}\right]^{z/d} \tag{24}$$

and

$$\mu(z) = \mu_O \left[\frac{\mu_m}{\mu_o}\right]^{z/d} \tag{25}$$

and then,

$$\frac{K_D(z)}{\mu(z)} = \left[\frac{K_o}{\mu_o}\right]\left[\frac{K_m}{\mu_m}\frac{\mu_o}{K_o}\right]^{z/d} \tag{26}$$

where $0 \le z \le d$ and the subscripts o and m, denoting initial and maximum values, represent, respectively, the property at the leading edge of the lattice (i.e., $\phi \sim 0.25$) and at the segregation where $\phi \sim 6$. When these are substituted into Eqn. 17,

$$\frac{\partial \bar{P}}{\partial z} + \overline{\Delta \rho g} = -V_z \frac{1}{d}\frac{\mu_o}{K_o} \int_0^d \left[\frac{K_o}{\mu_o}\frac{\mu_m}{K_m}\right]^{z/d} dz \tag{27}$$

and performing the integration yields

$$\frac{\partial \bar{P}}{\partial z} + \overline{\Delta \rho g} = -V_z \frac{1}{n}\frac{\mu_o}{K_o}\left[\frac{K_o}{\mu_o}\frac{\mu_m}{K_m} - 1\right], \tag{28}$$

where the constant $n = \ln(\mu_m K_o/\mu_o K_m)$. In the limit for constant properties, $\mu_m = \mu_o$ and $K_o = K_m$, $n \to 0$ as also does the term in brackets. This indeterminacy (i.e., 0/0) can be removed by recalling L'Hopital's rule for limits, whence Eqn. 28 reduces to the expected result for constant properties (i.e., Darcy's Law).

$$\frac{\partial \bar{P}}{\partial z} + \overline{\Delta \rho g} = -V_z \left[\frac{\mu}{K_D}\right]. \tag{29}$$

The more general condition for solidification fronts, $\mu_m/K_m \gg \mu_o/K_o$, reduces Eqn. 28, upon rearranging, to

$$V_m = -n \frac{K_m}{\mu_m}\left[\frac{\partial \bar{P}}{\partial z} + \overline{\Delta \rho g}\right]. \tag{30}$$

The flow is thus regulated by the largest viscosity and the smallest permeability occurring over the thickness d, which is immediately below the segregation. The numerical factor n, which could commonly be ~10, enhances the flow over the absolute minimum rate dictated by K_m/μ_m. The flow is governed, in effect, by constant properties over a thin region at the base of the segregation. The actual thickness of this region must scale with the thickness of the front itself, which increases with time. An estimate of this thickness can be made by finding the value of the exponent z/d in Eqn. 26 that is n times larger than K_m/μ_m, which is given by the solution of

$$\frac{K_o}{\mu_o}\left[\frac{K_m \mu_o}{\mu_m K_o}\right]^{z/d} = n\left[\frac{K_m}{\mu_m}\right] \tag{31}$$

for z/d, which is

$$\frac{z}{d} = 1 + \frac{\log(n)}{\log\left[\dfrac{K_m \mu_o}{\mu_m K_o}\right]}. \tag{32}$$

For $\log(n) \sim 1$ and $\log(K_m\mu_o/K_o\mu_m) \sim -5$, $z/d = 8/10$. This suggests that the effective layer thickness (δ) is ~2/10 of the thickness of the front below the segregation (i.e., $d(t)$) or ~1/10 of the full front thickness (i.e., $\sim h(t)/10$). This local layer regulating the flow filling the opening segregation hence has an effective thickness, $\delta(t)$, that can be defined by

$$\frac{\delta(t)}{d(t)} = 1 - \frac{z}{d(t)} \approx \frac{1}{5}. \tag{33}$$

And because $d(t) \sim h(t)/2$ and, from Eqn. 12, $h(t)$ increases with $(Kt)^{1/2}$, then $\delta(t)$ also increases as $(Kt)^{1/2}$, but more slowly than for h.

It is also useful to compare the thickness $\delta(t)$ controlling the porous flow to the thickness of the region supplying melt to the segregation. From conservation of mass, the supply region will have a thickness $\delta_s(t)$ relative to the thickness $S(t)$ of the segregation itself

$$\frac{\delta_s(t)}{S(t)} = \overline{(1-\phi)}^{-1}, \tag{34}$$

where the term in parentheses is the mean porosity in the supply region. This assumes that all of the melt is extracted to fill the tear, which may not be strictly true, and is thus a minimum estimate of the source thickness. Then, because the segregations form where $0.5 \le \phi \le 0.7$, $\delta_s(t)$ is at least two to three times thicker than the segregations themselves.

As mentioned much earlier, segregations generally thicken downward in sills, and the thicker the sill the thicker the segregations. First appearing near the roof as ~ 1-cm-thick lenses, they may become as large as 1 to 2 m at a depth of $\sim 0.15L$ to $0.25L$, where L is the full thickness of the sill, as long as the sill itself is >~250 m. This implies that the supply region is never more than ~1 to 6 m thick, and more typically less than ~0.1 to 1 m, depending on depth in the sill. Because from above, $\delta(t) \sim h(t)/10$, and the maximum $h(t) \sim L/4$ when the segregations form, where the sill thickness (L) is commonly 100 to 500 m, the maximum $\delta(t)$ is in the range of ~2 to 10 m. This is slightly larger, by a factor of ~2, but similar in size to $\delta_s(t)$. This suggests, then, that $\delta(t) \sim \delta_s(t)$; the supply region and the region controlling the porous flow are roughly similar

in thickness, but both are thin relative to the thickness of the leading, unstable part of the solidification front. This situation is shown schematically by Figure 8.

The flux of interstitial melt is thus driven by the pressure gradient

$$\overline{\frac{\partial P}{\partial z}} \approx -\frac{\overline{\Delta P}}{d} = -\frac{\overline{\Delta \rho_f} g d(t)}{d(t)} = -\frac{\overline{\Delta \rho_f} g h(t)}{2d(t)}, \tag{35}$$

and the flux of melt is given by the final form of Darcy's equation,

$$V_m(K_m, \mu_m, \Delta\rho^*, h/\delta) = n \frac{K_m}{\mu_m}\left[\frac{\overline{\Delta \rho_f} g h(t)}{2\delta(t)} + \overline{\Delta \rho} g\right], \tag{36}$$

where $\Delta\rho^*$ represents the two mean density contrasts $\Delta\rho_f$ and $\overline{\Delta\rho}$. If this flow is rapid enough, relative to the local advance of the front itself, a segregation will form.

5.6. Segregation Formation

A segregation forms when inflowing melt fills an opening tear before the local front can strengthen sufficiently through crystallization to preclude further tearing. Segregation formation is thus a competition between the rate of interstitial melt inflow and the rate of strengthening. If a tear of thickness S can fill with melt before the front stiffens enough locally to prevent tearing, a segregation will form. The characteristic time to fill a segregation of thickness $S(t)$ is

$$t = \frac{S(t)}{V_m(K_m, \mu_m, \Delta\rho^*, h/\delta)}, \tag{37}$$

where again $\Delta\rho^*$ represents the two mean density contrasts $\Delta\rho_f$ and $\overline{\Delta\rho}$.

A characteristic time of strengthening is given by the time taken for the solidus to propagate ahead a distance of $h(t)/2$ or $d(t)$. (This is somewhat of a liberal measure, but it can be easily relaxed without a great effect.) That is, from Eqn. 12 and Eqn. 14,

$$t_s = \frac{h(t)/2}{\partial h(t)/\partial t} = \frac{(2-b)}{b}\, t. \tag{38}$$

An estimate of the segregation thickness that can form under these conditions comes by setting these last two results equal to one another and solving for $S(t)$.

$$S(t) = V_m(K_m(e, a), \mu_m, \Delta\rho^*, h/\delta)\left[\frac{(2-b)}{b}\, t\right], \tag{39}$$

where the function V_m is given by Eqn. 36. Before solving for explicit values of $S(t)$, the various physical properties involved must be considered. Melt viscosity and density contrast, along with melt composition are readily available (e.g., MELTS; Lange and Carmichael, 1987; Ochs and Lange, 1997).

The least well known, yet critically important, parameter is the local permeability of the solidification front (K_m). Most permeability measurements of crystalline rocks involve the relatively low temperature flow of water through fractures (e.g., Brace, 1980) or of flow at small melt fractions where the degree of wetting of grain boundaries and considerations of dihedral angles are important (e.g., Watson, 1982). Here we want, instead, an estimate of permeability at large melt fractions in plagioclase-rich systems where extensive interconnected crystalline networks dominate. Such estimates are possible in mushy alloys and, despite the fact that they are usually dendritic, when they are fine grained these textures are broadly similar to rocks. Also, the dendritic character is a fair proxy for a plagioclase network structure. Measurements by Piwonka and Flemings (1966) cover a range of melt fraction of 0.1 to 0.9 in Al-Cu alloy, and measurements by Murakami and Okamoto (1984) in a granular alloy, simulated with a borneol-paraffin alloy, span a melt fraction range of ~0.25 to 0.55. In remarkable agreement with the threshold of critical crystallinity observed to control the eruption of magma (Marsh, 1981), the latter study found the solid assemblage to remain intact until the melt fraction reached 0.523 whereupon the solids desegregated or became fluidized. The data from both studies are shown by Figure 9, where also shown are estimates of permeability calculated from the Blake-Kozeny-Carman equation

$$K_D = \frac{a^2 e^3}{C_k(1-e)^2} \tag{40}$$

using the grain sizes of these materials and where C_k is a constant. This constant is usually taken to be 150 for granular materials, but for the present partially molten media a value of 100, assumed henceforth, fits these data much better.

There are many, perhaps fifty or more, formulas that have been suggested to describe permeability as a function of grain size, porosity, particle surface area, pore size, and tortuosity (e.g., German, 1989). Although most formulas show a direct proportion to the square of grain size and the cube of porosity, this particular relation Eqn. 40 has the attractive feature of permeability increasing dramatically as porosity increases beyond ~0.55, which is known to be so for igneous rocks (Marsh, 1981). Considering the inherent uncertainties in grain size in these data and the commonly found significant mismatch between predicted and measured permeabilities, the agreement here is satisfactory. Permeability in the solidification front is thus set by the local porosity and grain size, which is, strictly speaking, set by the local rates of nucleation and growth, a matter beyond the scope of the present work (but see Zieg and Marsh, 2002).

The segregation thickness can now be calculated from Eqn. 39 as a function of time after emplacement or also of the thickness of the solidification front. These results are shown by Figure 10 for six representative combinations of porosity, grain size (radius), density contrast, melt viscosity, and h/g. As might be expected, all properties that hasten the flow of interstitial melt (i.e., lower viscosity, larger grain size, larger density contrast, and lower crystallinity) produce thicker segregations earlier during solidification. But for any set of physical properties, segregations increase in size with depth in the sill. Segregations up to ~2 m thick can be expected in thick sills (i.e., 300 to 400 m), but if the interstitial melt is sufficiently viscous ($\sim 10^{4.5}$) or the crystallinity at failure too large ($>\sim$ 0.7) only thin (~0.25 m) segregations will form regardless of sill thickness. Moreover, because there is no explicit mecha-

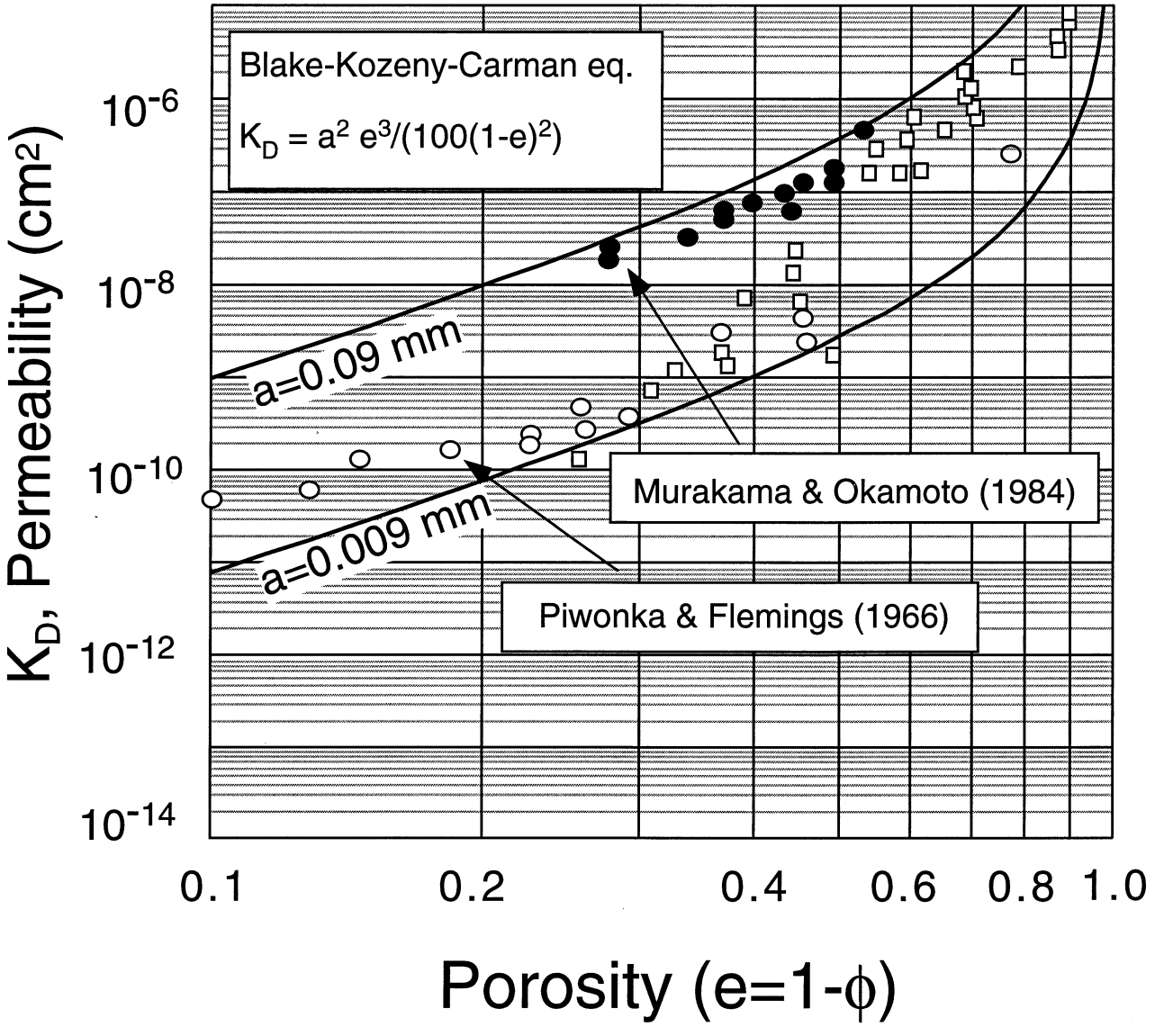

Fig. 9. Permeability measured as a function of crystallinity for two alloys (points) in comparison with the permeability predicted by the Blake-Kozeny-Carman equation.

nism in these calculations to stop the overall process of instability, with time or with the square of the front thickness (see upper axis) new segregations will be proportionally thicker. Segregations do thicken with depth in sills, but then thin and are absent beyond a certain depth, perhaps near 0.3*L*. This suggests that stress builds systematically during solidification, is sporadically released, and then subsides, perhaps due to the changing structural integrity of the front now containing segregations or perhaps due to the increasing proximity of the rising lower solidification front. That segregations often die out after formation of a 0.5- to 2-m thick segregation suggests stability may arise from the former cause. Once formed, the segregation acts as a buoyant layer, stabilizing the front and curtailing further porous flow. The fact that the entire front does not disengage and sink to the floor in sills is probably also attributable to the influence of the proximity of the basal front. In significantly thicker intrusions, like Skaergaard and Klokken, large blocks of the upper front, up to 1 km long and over 100 m thick, are found in the lower parts of the intrusion (e.g., McBirney and Noyes, 1979; Parsons and Becker, 1987). When this occurs pervasively, the segregated melt is free to move and collect at high points along the remaining solidification front, perhaps forming silicic masses of significant volume.

6. SFI SEGREGATIONS AND DIFFERENTIATION

The bulk composition of segregations is that of the local interstitial melt, the composition of which is governed by phase equilibria. The extraction of the melt appears chemically as a form of fractional crystallization. An equilibrium assemblage of crystals is removed from its resident interstitial melt. If an

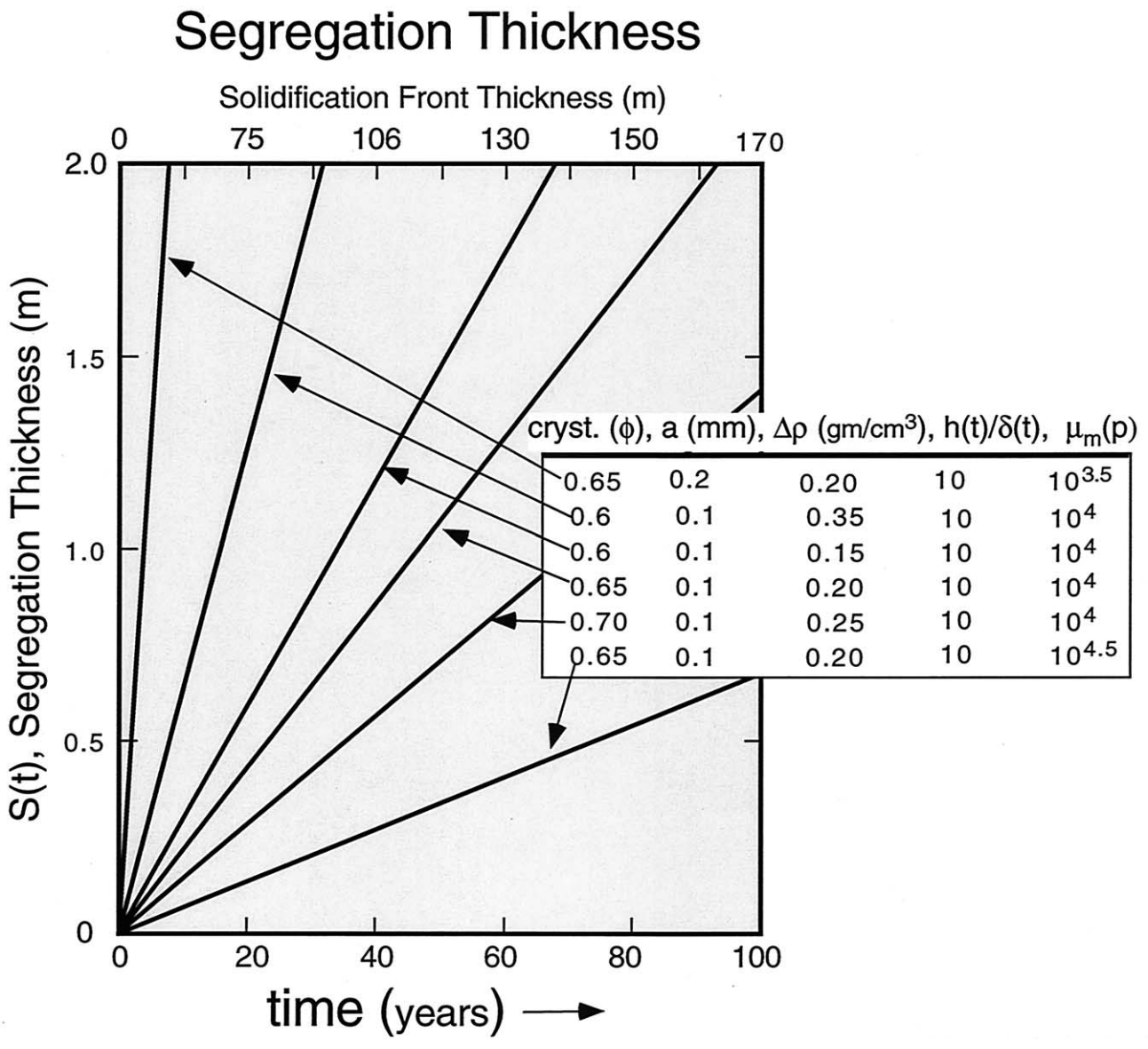

Fig. 10. Time (lower axis) necessary to form a segregation of up to 2 m in thickness (vertical axis) for a range of interstitial physical properties and crystallinities at the time of instability. The thickness of the upper solidification front at the time of instability is given along the upper axis.

ensemble of segregations were collected and erupted as lava, this mass would, in the light of all the usual gauges of magma evolution, appear to be a product of classical fractional crystallization. Thus, the appearance of siliceous lavas in a predominantly basaltic terrane may well suggest the operation of SFI.

The extent of silica enrichment for quartz normative magmas is determined by the crystallinity at the point of SFI, which is set by the strength of the crystalline matrix. For basaltic magmas SFI occurs, on the basis of mass balance chemistry, at ~60 to 70% crystals where the matrix has a strength of ~1 bar, and the segregated melt has a silica content ~8 to 10% (wt) greater than the host magma. Highly siliceous melt compositions (e.g., 70 to 75 wt% silica) occur too far back in the front to be accessible to this form of extraction. The crystalline matrix is much too strong to be vulnerable to SFI at the high crystallinities where rhyolitic melts exist (Fig. 2).

The more siliceous the initial magma the more siliceous the segregations. An initial magma of 55 wt% silica could produce lenses as silicic as 65 wt%. But there is a clear limit as to how siliceous the initial magma can be and still undergo SFI. That is, as the interstitial melt becomes highly siliceous, even at 60% crystals, the rate of melt flow may become too slow to form segregations. The use of Eqn. 39, for example, for melt viscosities of 10^5 and $10^{5.5}$ poise, the front would have to be ~550 m thick to form segregations of, respectively, 2.2 and 0.7 m thick. This would take ~1000 yr and the whole sheet would have to be ~2 km thick to persist over this length of time. Although this is clearly not unreasonable for large dacitic

intrusions, the net effect on differentiation is relatively small. The segregations form late and infrequently. The advantage of SFI in basaltic systems is that it operates efficiently and repeatedly in bodies of almost any size where other means of fractional crystallization are ineffective. Given a certain set of conditions, the process is unavoidable. In this context, it is a form of chaos. Once a set of necessary and sufficient physical and chemical conditions is achieved, the system splits both chemically and physically.

The vertical and horizontal variations in composition within a segregation may reflect the detailed process of infilling (Zavala and Marsh, 2001, and in preparation). As found above, the infilling melt is extracted from a zone two to three times thicker than the segregation itself. In old, thick fronts, melt composition will change slowly with distance below the segregation, so that even a 2-m-thick segregation could be relatively homogeneous in comparison to segregations forming in young, thin fronts where compositional gradients are larger. The most siliceous part of the segregation should be near its upper contact, and if the influx of melt has been uniform along the base of the tear, which is as yet unknown, thick segregations in young fronts may show significant compositional stratification. On the other hand, if the horizon of segregation formation is an interconnected, three-dimensional plexus of climbing and interdigitating tears, the compositional distribution within any single segregation may itself be complex both horizontally and vertically.

The local textures within segregations may also reflect the process of filling. Splotchy coarse or 'pegmatitic' areas within more even grained regions may indicate melt injected early in the filling process when crystal growth is less hindered. Early inflowing melt is derived immediately below the tear and will thus be in thermal and chemical equilibrium, which also favors larger crystals. Unusually large crystals are also favored by a general state of multiple saturation existing in this residual melt after 60 to 70% crystallization.

7. ROLE OF SFI IN THE DIFFERENTIATION OF BASALTIC MAGMAS

In most tholeiitic and calc-alkaline magmas, 50% crystallization increases the melt silica content by ~10 wt%. Regardless of whether fractionation is due to olivine, orthopyroxene, clinopyroxene, plagioclase, amphibole, or a combination thereof, the net effect is basically similar. At this degree of crystallinity, however, a crystalline matrix is present, for the solids are at maximum packing (Marsh, 1981), and separation of liquid and crystals is only possible by special processes like SFI. Crystal settling in the conventional sense is not possible. Not only does all crystallization take place within solidification fronts, crystal settling is possible only at crystallinities below ~30% where the melt is only ~2 or 3 wt% more siliceous than the initial magma. Crystals falling into the central, hotter region are small, sink slowly and dissolve into the magma (Jaeger and Joplin, 1955; Mangan and Marsh, 1992). Plumes of melt and crystals may perhaps fall from the upper solidification front (e.g., Marsh, 1988), but these simply join the lower front at a position equivalent to where they came from in the upper front. The net effect on differentiation is negligible.

The importance of SFI is that it irreversibly introduces, in essence, siliceous noise into basaltic systems in the form of lenses, pods, and local sheets. Any sheetlike intrusion yielding siliceous interstitial melts (e.g., quartz-normative magmas) can produce silicic segregations. Reconnaissance drilling in the Iceland crust, for example, shows that such features are relatively common in association with gabbroic intrusives (Armannsson et al., 1987). The occurrence of plagiogranite lenses in ophiolite sequences (e.g., Pallister and Hopson, 1981), which are clearly silicic segregations, also shows that these features are widespread in basaltic terranes. Yet the existence of these silicic segregations as disseminated features leaves the overall differentiation process incomplete unless they can be collected into viable siliceous plutons. This can obviously only occur through reprocessing.

Unlike at Hawaii and at most ocean ridges, in Iceland, spreading of the mid-Atlantic ridge, coupled with regionally enhanced magmatism, has produced a thickened basaltic crust of a strong bimodal, basaltic-rhyolitic, character. The absence of the requisite intermediate rocks produces the so-called Daly Gap (Daly, 1925). Silicic rocks make up some 10 to 12% of the volume of the surface rocks (Bunsen, 1851; Walker, 1966). The special tectonic feature of Iceland is that its crust undergoes systematic reprocessing through occasional jumping of the active spreading center to older crust, which leads to wholesale remelting of the crust. This allows collection of the silicic segregations into eruptible bodies of rhyolitic magma. The amassing of the segregations into viable magmas is driven by buoyancy and rapid compaction of the individual viscous blobs into a single mass. This process of remelting and collection is reflected in an abundance of telltale restitic debris in the rhyolites and oxygen isotopic signatures indicative of an origin as isolated bodies of silicic segregations that have been hydrothermally altered before melting (Gunnarsson et al., 1998). The lack of any similar extensive tectonic activity, fostering large scale reprocessing at typical ocean ridges and Hawaii, precludes the production of a significant flux of silicic magma that can lead to a bimodal crustal composition (Marsh et al., 1991). The small but persistent bimodal signal at many oceanic islands may, in general, indicate the operation of these two necessary processes, namely, SFI and systematic reprocessing (remelting) in the underlying volcanic pile and mush column. Reprocessing occurs through sustained volcanism over significant periods of time, generally millions of years, from a single volcanic center, which reflects a lack of strong tectonic mobility relative to the underlying magmatic source. The great mobility of volcanic centers like Hawaii and the immobility of the axial rift at ocean ridges (in a ridge reference frame) stifle reprocessing.

The specific process of reprocessing that allows production of silicic magma from disseminated siliceous pods is the breakdown of the host rock during melting, freeing fully molten viscous blobs, which can progressively collect at high points in the system. The critical property of the host rock that allows this to happen is the large spatial nonuniformity of melting temperature. That is, in compositionally heterogeneous country rock, the spatial pattern (e.g., contours) of any specific isotherm marking the structural breakdown of the mushy rock will be complex. But a local anomalous thermal field, spreading more or less uniformly outward from an intrusion, will produce a tortuous pattern of strength in the country rock. Given the opportunity the country rock will systematically collapse in-

ward as the anomalous thermal regime propagates outward. Fully molten blobs of siliceous melt are released to collect and compact into a viable mass within a plexus of mushy, more basaltic, country rock. To keep the process alive, which is in some ways akin to zone refining, the basaltic component must also undergo some form of compaction. There are also serious thermal constraints on the overall amount of processing that can be done for any given volume of intrusive (e.g., Bergantz and Dawes, 1994; Jackson and Cheadle, 1998). The proper thermal conditions are greatly favored by the high contact temperatures in the lower crust, which allows solidification fronts to become prograde (i.e., outward propagating) melting fronts.

This physical process of bimodal melt production is akin to reaching an invariant point in phase equilibria. Instead of the interstitial melt evolving smoothly in composition and volume with progressive crystallization or melting, the demands of invariance hold composition constant and allow only melt volume to change. In SFI, invariance is a spatial phenomenon. Local physical conditions allow melt to be concentrated under approximately isothermal conditions. Invariant points have long been attractive features to use to explain the occurrence of the preponderate magma types. Before much was known of the phase equilibria of magma, eutectic "pole" compositions were thought to dictate the major magma types (Marsh, 1996). In considering the problem of bimodality in lavas, Yoder (1973) gave a masterful analysis of the use of invariant points to produce compositional separation during partial melting of a uniform source rock. A similar argument was laid out by Bowen (1915) to show how basalt might fractionate to rhyolite. All approaches of this nature, however, rely critically on the melt being physically removed from the system at the appropriate time during compositional invariance. Many physical processes, the majority of which are probably physically untenable, have been suggested to extract and bring silicic and basic magmas together to explain occurrences of bimodality among lavas (see Yoder, 1973, for an especially useful review). When viewed in lavas or dikes, the overwhelming evidence for bimodality is the contemporaneous existence of significant volumes of contrasting compositions. Although of major importance, this fact alone offers little evidence of the physical process of compositional splitting. This evidence must come from the physical process itself as recorded by intrusives. It is this sector of the problem that has gone relatively unappreciated, presumably because it is difficult to read the evidence in outcrop for what it is. That is, the physical mass of individual segregations is small relative to any erupted volume of lava. Yet this is the critical silicic signal that is amplified through reprocessing to give rise to eruptible masses of silicic magma. Thus, the physical formation of compositional heterogeneity in otherwise uniform rock, regardless of scale, may be the key to the diversity of the igneous rocks.

Acknowledgments—Over the past 15 yr, this work on SFI has benefited greatly from in-depth discussions with a host of people in both the field and laboratory. These people include Matthias Hort, Michael Zieg, A. R. Philpotts, Karina Zavala, and Bjorn Gunnarsson, among many others. Conversations on flow in porous media with O. M. Phillips were enlightening. Some aspects of the general idea of SFI have been presented in the Hallimond Lecture (Marsh, 1996) and the Daly Lecture for 2000. Constructive and detailed reviews by two anonymous referees and especially Dougal Jerram were beneficial. This work is supported by the National Science Foundation Office of Polar Programs (OPP-9814332).

Associate editor: M. S. Ghiorso

REFERENCES

Anderson A. T. J., Swihart G. H., Artioli G., and Geiger C. (1984) Segregation vesicles, gas filter-pressing, and igneous differentiation. *J. Geol.* **92,** 55–72.

Armannsson H., Gudmundsson A., and Steingrimsson B. S. (1987) Exploration and development of the Krafla geothermal area. *Jokull* **37,** 13–30.

Arzi A. A. (1978) Critical phenomena in the rheology of partially melted rocks. *Tectonophysics* **44,** 173–184.

Bergantz G. W. and Dawes R. (1994) Aspects of magma generation and ascent in continental lithosphere. In *Magmatic Systems* (ed. M. Ryan), pp. 291–317. Academic Press.

Bowen N. L. (1910) Diabase and granophyre of the Gowganda Lake District, Ontario. *J. Geol.* **18,** 658–674.

Bowen N. L. (1915a) The later stages of the evolution of the igneous rocks. *Journal of Geology* **23,** 1–89.

Brace W. F. (1980) Permeability of crystalline ans argillaceous rocks. *Int. J. Rock Mechanics Mining Sci.* **17,** 241–251.

Bunsen R. W. (1851) Uber die. Processe der vulkanischen Gesteinbildungen Islands. *Ann Phys Chem.* **83,** 197–272.

Carman Jr. M. F. (1994) Mechanisms of differentiation in shallow mafic alkaline intrusions, as illustrated in the Big Bend area, western Texas. *J. Volcanol. Geothermal Res.* **61,** 1–44.

Caroff M., Ambrics C., Maury R. C., and Cotten J. (1997) From alkali basalt to phonolite in hand-size samples: vapor-differentiation effects in the Bouzentes lava flow (Cantal, France). *J. Volcanol. Geothermal Res.* **79,** 47–61.

Carrigan C. R. (1986) A two-phase hydrothermal cooling model for shallow intrusions. *J. Volcanol. Geothermal Res.* **28,** 175–192.

Carrigan C. R. (1988) The Biot number and the "Thermos bottle" effect: Implications for magma chamber convection. *Geology* **16,** 771–774.

Carslaw H. S. and Jaeger J. C. (1959) *Conduction of Heat in Solids.* Clarendon Press.

Daly R. A. (1925) The geology of Ascension Island. *Proc. Am. Acad. Arts Sci.* **60,** 1–80.

Delaney P. T. (1988) Fortran 77 Programs for conductive cooling of dikes with temperature-dependent thermal properties and heat of crystallization. *Comp. Geosci.* **14,** 181–212.

German R. M. (1989) *Particle Packing Characteristics*. Metal Powder Industries Federation.

Ghiorso M. S. (1991) Temperatures in and around cooling magma bodies. In *Progress in Metamorphic and Magmatic Petrology* (ed. L. L. Perchuk), pp. 387–410. Cambridge University Press.

Ghiorso M. S. and Carmichael I. S. E. (1987) Modeling magmatic systems: Petrologic applications. In *Thermodynamic Modeling of Geological Materials: Minerals, Fluids and Melts, Vol. 17* (eds. I. S. E. Carmichael and H. P. Eugster), pp. 467–499. Mineralogical Society of America.

Goff F. (1996) Vesicle cylinders in vapor-differentiated basalt lavas. *J. Volcanol. Geothermal Res.* **71,** 167–185.

Gunn B. M. (1966) Modal and element variation in Antarctic tholeiites. *Geochim. Cosmochim. Acta* **30,** 881–920.

Gunnarsson B., Marsh B. D., and Taylor Jr. H. P. (1998) Generation of Icelandic rhyolites: Silicic lavas from the Torfajokull central volcano. *J. Volcanol. Geothermal Res.* **83,** 1–45.

Helz R. T. (1980) Crystallization history of Kilauea Iki lava lake as seen in drill core recovered in 1967–1979. *Bull. Volcanol.* **43,** 675–701.

Helz R. T. and Thornber C. R. (1987) Geothermometry of Kilauea Iki lava lake, Hawaii. *Bull. Volcanol.* **49,** 651–668.

Helz R. T., Kirschenbaum H., and Marinenko J. W. (1989) Diapiric transfer of melt in Kilauea Iki lava lake, Hawaii: A quick, efficient process of igneous differentiation. *Geol. Soc. Am. Bull.* **101,** 578–594.

Hort M., Marsh B. D., Resmini R. G., and Smith M. K. (1999) Convection and crystallization in a liquid cooled from above: An experimental and theoretical study. *J. Petrol.* **40,** 1271–1300.

Hurlbut C. S. J. (1939) Igneous rocks of the Highwood Mountains, Montana, part I: The Laccoliths. *Bull. Geol. Soc. Am.* **50,** 1043–1112.

Jackson M. D. and Cheadle M. J. (1998) A continuum model for the transport of heat, mass, and momentum in a deformable, multicomponent mush undergoing solid–liquid phase change. *Int. J. Heat Mass Transfer* **41,** 1035–1048.

Jaeger J. C. (1957) The solidification and cooling of intrusive sheets. In *Dolerite: A Symposium* (ed. S. W. Carey), pp. 77–87. University of Tasmania, Hobart.

Jaeger J. C. (1968) Cooling and solidification of igneous rocks. In *Basalts: The Poldervaart Treatise on Rocks of Basaltic Composition, Vol. 2* (eds. H. H. Hess and A. Poldervaart), pp. 503–536. Interscience.

Jaeger J. C. and Joplin G. A. (1955) Rock magnetism and the differentiation of dolerite sills. *J. Geol. Soc. Aust.* **2,** 1–19.

Jaeger J. C. and Cook N. G. W. (1979) *Fundamentals of Rock Mechanics*. Chapman and Hall.

Lane A. C. (1898) Geological report on Isle Royale. *Geol. Survey Michigan* **6,** 106–121.

Lange R. A. and Carmichael I. S. E. (1987) Densities of Na_2O-K_3O-CaO-MgO-FeO-Fe_2O_3-Al_2O_3-TiO_2-SiO_2 liquids: New measurements and derived partial molar properties. *Geochim. Cosmochim. Acta* **51,** 2931–2946.

Lindsley D. H., Smith D., and Haggerty S. E. (1970) Petrography and mineral chemistry of a differentiated flow of picture gorge basalt near Spray, Oregon. *Carnegie Inst. Year Book,* 264–359.

Long P. E. and Wood B. J. (1986) Structures, textures, and cooling histories of Columbia River basalt flows. *Geol. Soc. Am. Bull.* **97,** 1144–1155.

MacLeod N. S. (1981) *Differentiation of a Gabbro Sill in the Oregon Coast Range by Crystallization-Zone Settling*. U.S. Geological Survey Professional Paper 1165.

Mangan M. T. and Marsh B. D. (1992) Solidification front fractionation in phenocryst-free sheet-like magma bodies. *J. Geol.* **100,** 605–620.

Mangan M. T., Marsh B. D., Froelich A. J., and Gottfried D. (1993) Emplacement and differentiation of the York Haven Diabase Sheet, Pennsylvania. *J. Petrol.* **34,** 1271–1302.

Marsh B. D. (1981) On the crystallinity, probability of occurrence, and rheology of lava and magma. *Contrib. Mineral. Petrol.* **78,** 85–98.

Marsh B. D. (1988) Crystal capture, sorting, and retention in convecting magma. *Geol. Soc. Am. Bull.* **100,** 1720–1737.

Marsh B. D. (1989a) Magma Chambers. In *Annual Review of Earth and Planetary Sciences, Vol. 17* (eds. G. W. Wetherill, A. L. Albee, and F. G. Stehli), pp. 439–474. Annual Reviews.

Marsh B. D. (1989b) On convective style and vigor in sheet-like magma chambers. *J. Petrol.* **30,** 479–530.

Marsh B. D.(1991) Solidification front instability (SFI) and silicic chaos in basaltic magma chambers. Geological Society of America (abstract). **23**, A270.

Marsh B. D. (1996) Solidification fronts and magmatic evolution. *Mineral. Mag.* **60,** 5–40.

Marsh B. D., Gunnarsson B., Congdon R., and Carmody R. (1991) Hawaiian basalt and Icelandic rhyolite: Indicators of differentiation and partial melting. *Geol. Rundschau* **80,** 481–510.

McBirney A. R. and Noyes R. M. (1979) Crystallization and layering of the Skaergaard Intrusion. *J. Petrol.* **20,** 487–554.

Moore J. G. and Evans B. W. (1967) The role of olivine in the crystallization of the prehistoric Makaopuhi tholeiitic lava lake, Hawaii. *Contrib. Mineral. Petrol.* **15,** 202–223.

Murakami K. and Okamoto T. (1984) Fluid flow in the mushy zone composed of granular grains. *Acta metall.* **32**(10)**,** 1741–1744.

Ochs F. A. I. and Lange R. A. (1997) The partial molar volume, thermal expansivity, and compressibility of H_2O in silicate melts: New measurements and an internally consistent model. *Contrib. Mineral. Petrol.* **129,** 155–165.

Pallister J. S. and Hopson C. A. (1981) Samail ophiolite plutonic suite: Field relations, phase variation, cryptic variation and layering, and a model of a spreading ridge magma chamber. *J. Geophys. Res.* **86,** (B4) 2593–2644.

Parsons I. and Becker S. M. (1987) Layering, compaction and postmagmatic processes in the Klokken Intrusion. In *Origins of Igneous Layering* (ed. I. Parsons), pp. 29–92. Reidel.

Peck D. L., Hamilton M. S., and Shaw H. R. (1977) Numerical analysis of lava lake cooling models: Part II, application to Alae Lava Lake, Hawaii. *Am. J. Sci.* **277,** 415–437.

Peterson D. W. and Moore R. B. (1987) Geologic history of evolution of geologic concepts, Island of Hawaii. In *Volcanism in Hawaii, Vol. 1* (eds. R. W. Decker, T. L. Wright, and P. H. Stauffer), pp. 149–190. U.S. Government Printing Office.

Phillips O. M. (1991) *Flow and Reactions in Permeable Rocks*. Cambridge University Press.

Philpotts A. R. and Carroll M. (1996) Physical properties of partly melted tholeiitic basalt. *Geology* **24,** 1029–1032.

Philpotts A. R., Carroll M., and Hill J. M. (1996) Crystal-mush compaction and the origin of pegmatitic segregation sheets in a thick flood-basalt flow in the Mesozoic Hartford Basin, Connecticut. *J. Petrol.* **37,** 811–836.

Piwonka T. S. and Flemings M. C. (1966) Pore formation in solidification. *Transactions of the Metallurgical Society of AIME* **236,** 1157–1165.

Puffer J. H. and Horter D. L. (1993) Origin of pegmatitic segregation veins within flood basalts. *Geol. Soc. Am. Bull.* **105,** 738–748.

Renner J., Evans B., and Hirth G. (2000) On the rheologically critical melt fraction. *Earth Planet. Sci. Lett.* **181,** 585–594.

Richter D. H., Moore J. G.(1966) Petrology of the Kilauea Iki Lava Lake Hawaii. U.S. Geological Survey Professional Paper 537-B.

Ryerson F. J., Weed H. C., and Piwinskii A. J. (1988) Rheology of subliquidus magmas, 1. Picritic compositions. *J. Geophys. Res.* **93,** (B4) 3421–3436.

Schultz R. A. (1993) Brittle strength of basaltic rock masses with applications to Venus. *J. Geophys. Res.* **98,** (E6) 10883–10895.

Shaw H. R. (1969) Rheology of basalt in the melting range. *J. Petrol.* **10,** 510–535.

Shaw H. R. (1980) The fracture mechanisms of magma transport from the mantle to the surface. In *Physics of Magmatic Processes* (ed. R. B. Hargraves), pp. 201–264. Princeton University Press.

Sleep N. H. (1988) Tapping of Melt by Veins and Dikes. *J. Geophys. Res.* **93,** (B9) 10255–10272.

Sonnenthal E. L.(1990) Part I. Matasomatic replacement and the behavior of fluorine and chlorine during differentiation of the Skaergaard intrusion, East Greenland. Part II. Geochemical and physical aspects of melt segregation in the Picture Gorge Basalt, Oregon. Ph.D. dissertation. University of Oregon.

Timoshenko S. (1940) *Strength of Materials Part 1: Elementary Theory and Problems*. D. Van Nostrand.

Tomkeieff S. I. (1940) The basalt lavas of the Giant's Causeway district of Northern Ireland. *Bull. Volcanol.* **6–7,** 89–146.

Turcotte D. L. and Schubert G. (1982) *Geodynamics*. Wiley.

van der Molen I. and Paterson M. S. (1979) Experimental deformation of partially-melted granite. *Contrib. Mineral. Petrol.* **70,** 299–318.

Walker F. (1953) The pegmatitic differentiates of basic sheets. *Am. J. Sci.* **251,** 41–60.

Walker G. P. L. (1966) Acid volcanic rock in Iceland. *Bull. Volcanol.* **29,** 375–402.

Walker F. and Poldervaart A. (1949) Karroo dolerites of the Union of South Africa. *Geol. Soc. Am. Bull.* **60,** 591–706.

Watson E. B. (1982) Melt infiltration and magma evolution. *Geology* **10,** 236–240.

Wheelock M. M. and Marsh B. D. (1993) Bimodal differentiation: Silicic segregations in the Ferrar Dolerites. *Antarctic J. United States* **29,** 19–21.

Wright T. L. and Okamura R. T. (1977) *Cooling and Crystallization of Tholeiitic Basalt, 1965 Makaopuhi Lava Lake, Hawaii* Professional Paper 1004. U.S. Geological Survey.

Yoder Jr. H. S. (1973) Contemporaneous basaltic and rhyolitic magmas. *Am. Mineral.* **58,** 153–171.

Zavala K. and Marsh B. D. (2000) On silicic segregations a physical and chemical link of basaltic to rhyolite (abstract). *EOS Trans. Am. Geophys. Union* **81,** 435.

Zavala K. and Marsh B. D. (2001) On the filling process forming silicic segregations (abstract). *Trans. Am. Geophys. Union.* **82,** 432.

Zieg M. J. and Marsh B. D. (2002) Crystal size distributions and scaling laws in the quantification of igneous textures. *J. Petrol.* **43,** 85–101.